

Stochastic excitation of acoustic modes in stars

R. Samadi

Observatoire de Paris, LESIA, CNRS UMR 8109, 92195, Meudon, France

Abstract. For more than ten years, solar-like oscillations have been detected and frequencies measured for a growing number of stars with various characteristics (e.g. different evolutionary stages, effective temperatures, gravities, metal abundances ...).

Excitation of such oscillations is attributed to turbulent convection and takes place in the uppermost part of the convective envelope. Since the pioneering work of Goldreich & Keeley (1977), more sophisticated theoretical models of stochastic excitation were developed, which differ from each other both by the way turbulent convection is modelled and by the assumed sources of excitation. We review here these different models and their underlying approximations and assumptions.

We emphasize how the computed mode excitation rates crucially depend on the way turbulent convection is described but also on the stratification and the metal abundance of the upper layers of the star. In turn we will show how the seismic measurements collected so far allow us to infer properties of turbulent convection in stars.

1 Introduction

Solar p -modes are known to have finite lifetimes (a few days) and very low amplitudes (a few cm/s in velocity and a few ppm in intensity). Their finite lifetimes result from several complex damping processes that are so far not clearly understood. Their excitation is attributed to turbulent convection and takes place in the upper-most part of the Sun, which is the place of vigorous and turbulent motions. Since the pioneering work of Lighthill (1952), we know that a turbulent medium generates incoherent acoustic pressure fluctuations (also called acoustic “noise”). A very small fraction of the associated kinetic energy goes into the normal modes of the solar cavity. This small amount of energy then is responsible for the small observed amplitudes of the solar acoustic modes (p modes).

In the last decade, solar-like oscillations have been detected in numerous stars, in different evolutionary stages and with different metallicity (see recent review by Bedding & Kjeldsen 2007). As in the Sun, these oscillations have rather small amplitudes and have finite lifetimes. The excitation of such solar-like oscillations is attributed to turbulent convection and takes place in the outer layers of stars having a convective envelope.

Measuring mode amplitudes and the mode lifetimes permits us to infer \mathcal{P} , the energy supplied per unit time into the acoustic modes. Deriving \mathcal{P} puts constraints on the theoretical models of mode excitation by turbulent convection (Libbrecht 1988). However, as pointed-out by Baudin et al. (2005), even for the

Sun, inferring \mathcal{P} from the seismic data is not a trivial task. For stellar seismic data, this is even more difficult (Samadi et al. 2008). We discuss here the problems we face in deriving reliable seismic constraints on \mathcal{P} .

A first attempt to explain the observed solar five minute oscillations was carried out by Unno & Kato (1962). They have considered monopole¹ and dipole² source terms that arise from an isothermal stratified atmosphere. Stein (1967) has generalised Lighthill (1952)'s approach to a stratified atmosphere. He found that monopole source terms have a negligible contribution to the noise generation compared to the quadrupole source term³. Among the quadrupole source terms, the Reynolds stress was expected to be the major source of acoustic *wave* generation. It was only at the beginning of the 1970's that solar five minutes oscillations have been clearly identified as global resonant modes (Ulrich 1970; Leibacher & Stein 1971; Deubner 1975). A few years later, Goldreich & Keeley (1977b, GK hereafter) have proposed the first theoretical model of stochastic excitation of acoustic *modes* by the Reynolds stress. Since this pioneering work, different improved models have been developed (Dolginov & Muslimov 1984; Balmforth 1992a; Goldreich et al. 1994; Samadi & Goupil 2001; Chaplin et al. 2005; Samadi et al. 2003a; Belkacem et al. 2006b, 2008). These approaches differ from each other either in the way turbulent convection is described or by the excitation process.

In the present paper, we briefly review the different main formulations and discuss the main assumptions and approximations on which these models are based. As shown by Samadi et al. (2003a), the energy supplied per time unit to the modes by turbulent convection crucially depends on the way eddies are temporally correlated. A realistic modeling of the eddy time-correlation at various scale lengths then is an important issue, which is discussed in detail here. We will also highlight how the mean structure and the chemical composition of the upper convective envelope influence the mode driving. Finally, we will summarize how the seismic measurements obtained so far from the ground allow us to distinguish between different dynamical descriptions of turbulent convection.

2 Mode energy

We will show below how the energy of a solar-like oscillation is related to the driving and damping process. The mode total energy (potential plus kinetic) is by definition the quantity:

$$E_{\text{osc}}(t) = \int d^3x \rho_0 \mathbf{v}_{\text{osc}}^2(\mathbf{r}, t) \quad (1)$$

where \mathbf{v}_{osc} is the mode velocity at the position \mathbf{x} , and ρ_0 the mean density.

¹ A monopole term is associated with a fluctuation of density

² A dipole term is associated with a fluctuation of a force

³ A quadrupole term is associated with a shear

Mode damping occurs over a time-scale much longer than that associated with the driving. Accordingly, damping and driving can be completely decoupled in time. Furthermore, we assume a constant and linear damping such that

$$\frac{d\mathbf{v}_{\text{osc}}(t)}{dt} = -\eta \mathbf{v}_{\text{osc}}(t) \quad (2)$$

where η is the (constant) damping rate. The time derivative in Eq. (2) is performed over a time scale much larger than the characteristic time over which the driving occurs.

Let \mathcal{P} be the amount of energy injected per unit time into a mode by an arbitrary source of driving (which acts over a time scale much shorter than $1/\eta$). According to Eqs. (1) and (2), the variation of E_{osc} with time is given by:

$$\frac{dE_{\text{osc}}}{dt}(t) = \mathcal{P} - 2\eta E_{\text{osc}}(t). \quad (3)$$

Solar-like oscillations are known to be stable modes. As a consequence, their energy cannot growth on a time scale much longer than the time scales associated with the damping and driving process. Accordingly, averaging Eq. (3) over a long time scale gives:

$$\overline{\frac{dE_{\text{osc}}}{dt}}(t) = 0, \quad (4)$$

where $\overline{(\)}$ refer to a time average. From Eqs. (3) and (4), we immediately derive:

$$\overline{E}_{\text{osc}} = \frac{\overline{\mathcal{P}}}{2\eta}. \quad (5)$$

We then clearly see with Eq. (5) that a stable mode has its energy (and thus its amplitude) controlled by the balance between the driving (\mathcal{P}) and the damping (η). Then, the major difficulties are to model the processes that are at the origin of the driving and the damping. For ease of notation, we will drop from now on the symbol $\overline{(\)}$ from E_{osc} and \mathcal{P} .

3 Seismic constraints

As we shall see later, the mode displacement, $\delta\mathbf{r}_{\text{osc}}$, can be written in terms of the adiabatic eigen-displacement $\boldsymbol{\xi}$, and an instantaneous amplitude $A(t)$:

$$\delta\mathbf{r}_{\text{osc}} \equiv \frac{1}{2} (A(t) \boldsymbol{\xi}(\mathbf{r}) e^{-i\omega_{\text{osc}}t} + cc) \quad (6)$$

where cc means complex conjugate, ω_{osc} is the mode eigenfrequency, and $A(t)$ is the instantaneous amplitude resulting from both the driving and the damping. Note that, since the normalisation of $\boldsymbol{\xi}$ is arbitrary, the actual *intrinsic* mode

amplitude is fixed by the term $A(t)$, which remains to be determined. The mode velocity, \mathbf{v}_{osc} , is then given by:

$$\mathbf{v}_{\text{osc}}(\mathbf{r}, t) = \frac{d\delta\mathbf{r}_{\text{osc}}}{dt} = \frac{1}{2}(-i\omega_{\text{osc}} A(t) \boldsymbol{\xi}(\mathbf{r}) e^{-i\omega_{\text{osc}} t} + cc) \quad (7)$$

where cc means complex conjugate. Note that we have neglected in Eq. (7) the time derivative of A . This is justified since the mode period ($2\pi/\omega_{\text{osc}}$) is in general much shorter than the mode lifetime ($\sim 1/\eta$)

From Eqs. (7) and (1), we derive the expression for the mean mode energy:

$$E_{\text{osc}} = \int d^3x \rho_0 \overline{\mathbf{v}_{\text{osc}}^2} = \frac{1}{2} \overline{|A|^2} I \omega_{\text{osc}}^2, \quad (8)$$

where

$$I \equiv \int_0^M d^3x \rho_0 \boldsymbol{\xi}^* \cdot \boldsymbol{\xi} \quad (9)$$

is the mode inertia. For the sake of simplicity, we will from now on only consider radial modes. According to Eq. (7), the mean-square surface velocity associated with a *radial* mode measured at the radius r_h , is then given by the relation

$$\mathbf{v}_s^2(r_h) = \frac{1}{2} \overline{|A|^2} \omega_{\text{osc}}^2 |\xi_r(r_h)|^2 \quad (10)$$

where ξ_r is the radial component of the mode eigenfunction. It is convenient and common to define the mode mass as the quantity:

$$\mathcal{M}(r_h) \equiv \frac{I}{|\xi_r(r_h)|^2} \quad (11)$$

where r_h is the radius in the atmosphere where the mode is measured in velocity. According to Eqs. (8), (10), and (11), we derive the following relation:

$$E_{\text{osc}} = \mathcal{M} \mathbf{v}_s^2 \quad (12)$$

It should be noticed, that although \mathcal{M} and v_s depend on the choice for the radius r_h , E_{osc} is by definition intrinsic to the mode (see Eq. (1)) and hence is independent of r_h .

Using Eqs. (5), and (12), we finally derive:

$$\mathbf{v}_s^2(r_h, \omega_{\text{osc}}) = \frac{\mathcal{P}}{2\pi \mathcal{M} \Gamma} \quad (13)$$

where $\Gamma = \eta/\pi$ is the mode linewidth, and η the mode damping rate. From Eq. (13), one again sees that the mode surface velocity is the result of the balance between excitation (\mathcal{P}) and the damping ($\eta = \Gamma\pi$). However, it also depends on the mode mass (\mathcal{M}): For a given driving (\mathcal{P}) and damping (Γ), the larger the mode mass (or the mode inertia), the smaller the mode velocity.

When the frequency resolution and the signal-to-noise are high enough, it is possible to resolve the mode profile and then to measure *both* Γ and the mode

height H in the power spectral density (generally given in m^2/Hz). In that case v_s is given by the relation (see e.g. Baudin et al. 2005):

$$v_s^2(r_h, \omega_{\text{osc}}) = \pi C_{\text{obs}} H \Gamma \quad (14)$$

where the constant C_{obs} takes the observational technique and geometrical effects into account (see Baudin et al. 2005). From Eq. (13) and (14), one can then infer from the observations the mode excitation rates (\mathcal{P}) as:

$$\mathcal{P}(\omega) = 2\pi \mathcal{M} \Gamma v_s^2 = 2\pi^2 \mathcal{M} C_{\text{obs}} H \Gamma^2. \quad (15)$$

Provided that we can measure Γ and H , it is then possible to constraint \mathcal{P} . However, we point out that the derivation of \mathcal{P} from the observations is also based on models since \mathcal{M} is required. Furthermore, there is a strong anti-correlation between H and Γ (see e.g. Chaplin et al. 1998; Chaplin & Basu 2008) that can introduce important bias. This anti-correlation vanishes when considering the squared mode amplitude, v_s^2 , since $v_s^2 \propto H \Gamma$ (see Eq. (14)). However, \mathcal{P} still depends on Γ , which is strongly anti-correlated with H .

As an alternative to comparing theoretical results and observational data, Chaplin et al. (2005) proposed to derive H from the theoretical excitation rates, \mathcal{P} , and the observed mode line width, Γ , according to the relation:

$$H = \frac{\mathcal{P}}{2\pi^2 \mathcal{M} C_{\text{obs}} \Gamma^2} \quad (16)$$

However, as pointed-out by Belkacem et al. (2006b), H strongly depends on the observation technique. The quantity $C_{\text{obs}} H$, is less dependent on the observational data but still depends on the instrument since different instruments probe different layers of the atmosphere (see below). Therefore, one has difficulty to compare values of $H C_{\text{obs}}$ coming from different instruments.

3.1 Solar seismic constraints

Baudin et al. (2005) have inferred the solar p -mode excitation rates from different instruments, namely GOLF on-board SOHO, the BiSON and GONG networks. As pointed out by Baudin et al. (2005), the layer (r_h) where the mode mass is evaluated must be properly estimated to derive correct values of the excitation rates from Eq. (15). Indeed solar seismic observations in Doppler velocity are usually measured from a given spectral line. The layer where the oscillations are measured then depends on the height (r_h) in the atmosphere where the line is formed. Different instruments use different solar lines and then probe different regions of the atmosphere. For instance, the BiSON instruments use the KI line whose height of formation is estimated at the optical depth $\tau \approx 0.013$. The optical depth associated with the different spectral lines used in helioseismology are given in Houdek (2006) with associated references.

Solar p -mode excitation rates, \mathcal{P} , derived by Baudin et al. (2005) are shown in Fig. 1 (left panel). For $\nu \lesssim 3.2$ mHz, $\mathcal{P}^{\text{GONG}}$ and $\mathcal{P}^{\text{BiSON}}$ are consistent with

each other, whereas $\mathcal{P}^{\text{GOLF}}$ is systematically smaller than $\mathcal{P}^{\text{GONG}}$ and $\mathcal{P}^{\text{BiSON}}$, although the discrepancy remains within $1\text{-}\sigma$. At high frequency, differences between the different data sets are more important. This can be partially attributed to the choice of the layers r_h where \mathcal{M} are evaluated. Indeed, the sensitivity of \mathcal{M} to r_h is the larger at high frequency. On the other hand, low-frequency mode masses are much less sensitive to the choice of r_h . Accordingly, the discrepancy seen at low frequency between GOLF and the other data sets suggests that the absolute calibration of the GOLF data may not be correct (see Baudin et al. 2005). In Fig. 1, we then present \mathcal{P} derived from GOLF data after multiplying them by a factor in order that they match at low frequency $\mathcal{P}^{\text{GONG}}$ and $\mathcal{P}^{\text{BiSON}}$. We find a rather good agreement between $\mathcal{P}^{\text{GOLF}}$ and $\mathcal{P}^{\text{BiSON}}$ whereas, at high frequency, $\mathcal{P}^{\text{GONG}}$ are systematically lower than $\mathcal{P}^{\text{GOLF}}$ or $\mathcal{P}^{\text{BiSON}}$. The residual high-frequency discrepancy is likely due to an incorrect determination of the layer r_h where the different seismic measurements originate (see a detailed discussion in Baudin et al. 2005).

3.2 Stellar seismic constraints

Seismic observations in Doppler velocity of solar-like pulsators are performed using spectrographs dedicated to stellar seismic measurements (e.g. UCLES, UVES, HARPS). Such spectrographs use a large number of spectral lines in order to reach a high enough signal-to-noise ratio. In the case of stellar seismic measurements, it is then more difficult than for helioseismic observations to estimate the effective height r_h . As discussed in detail in Samadi et al. (2008), the computed mode surface velocities, v_s , depend significantly on the choice of the height, h , in the atmosphere where the mode masses are evaluated. This is illustrated in Fig. 2 for the case of the star α Cen A.

A recent work by Kjeldsen et al. (2008) allows us to estimate the value for an effective r_h . Indeed, the authors have found that solar modes measured with the UCLES spectrograph have amplitudes slightly smaller than those measured by the BiSON network. The instruments of the BiSON network use the potassium (K) resonance line, which is formed at an optical depth $\tau_{500\text{ nm}} \simeq 0.013$. Kjeldsen et al. (2008)'s results then suggest that acoustic modes measured by UCLES or an equivalent spectrograph (e.g. HARPS) are measured at an effective height (r_h) slightly below the formation depth of the K line, i.e. at optical depth slightly above $\tau_{500\text{ nm}} \simeq 0.013$. Accordingly, in the case of stellar seismic observations we will evaluate the mode masses at that optical depth. A more rigorous approach would be to compute an effective mode mass by weighting appropriately the different mode masses associated with the different spectral lines that contribute to the seismic measure. In order to infer accurate mode excitation rates from the stellar seismic data, the mode masses representative of the observation technique *and* the spectral lines of the observed star must be derived. However, this calls for further studies.

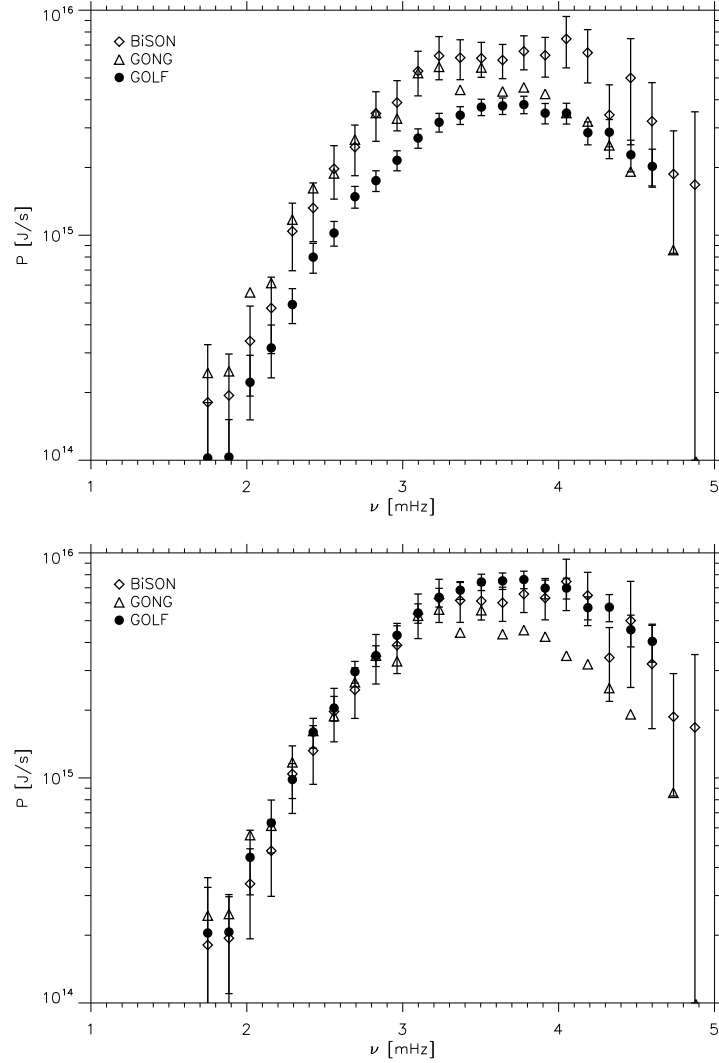


Fig. 1. **Left:** Solar p -mode excitation rates, \mathcal{P} , as a function of frequency and derived from different instruments. The filled circles correspond to seismic data from SOHO/GOLF, the diamonds to seismic data from the BiSon network, and the triangles to seismic data from the GONG network. **Right:** Same as left panel. \mathcal{P} derived from GOLF data multiplied by a factor in order that they match at low frequency the \mathcal{P} derived from GONG or BiSON.

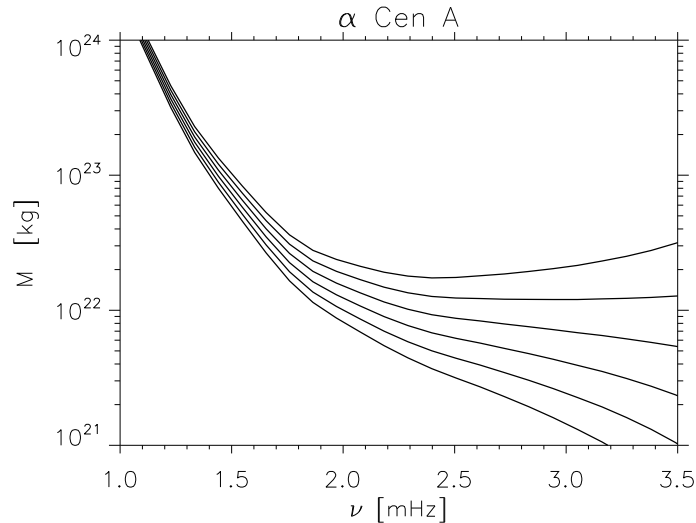


Fig. 2. Mode mass evaluated for the case of α Cen A at different heights h above the photosphere. The upper curve corresponds to the photosphere ($h = 0$) and the lower curve to the top of the atmosphere ($h = 1000$ km). The step in h is 200 km.

4 Theoretical models

4.1 The inhomogeneous wave equation

Most of the theoretical models of stochastic excitation adopt GK's approach. It consists to solve first, with appropriate boundary conditions, the equation that governs the *adiabatic* wave propagation (also called the homogeneous wave equation). This provides the well-known adiabatic displacement eigenvectors ($\xi(\mathbf{r}, t)$). Then, we include in the wave equation of propagation turbulent sources of driving as well as a linear damping. The complete equation (so-called inhomogeneous wave equation) is then solved and the solution corresponds to the forced mode displacement, $\delta\mathbf{r}_{\text{osc}}(\mathbf{r}, t)$ (or equivalently the oscillation mode velocity $\mathbf{v}_{\text{osc}} = d\delta\mathbf{r}_{\text{osc}}/dt$).

A detailed derivation of the solution can be found in Samadi & Goupil (2001, SG hereafter) or in Chaplin et al. (2005). We recall below the main steps.

Equilibrium quantities are represented with a subscript 0. Each variable f , except for the velocity \mathbf{v} , is written as the sum of the equilibrium quantity, f_0 and an Eulerian fluctuation, f_1 , $f = f_0 + f_1$ and we retain terms which are linear and quadratic in the variables P_1 and ρ_1 and neglect, g_1 , the gravitational perturbation⁴. Accordingly, one obtains for the perturbed momentum

⁴ Neglecting the perturbation of the gravity corresponds to Cowling (1941)'s approximation. This approximation remains valid for modes with a high n radial order.

and continuity equations:

$$\frac{\partial \rho \mathbf{v}}{\partial t} + \nabla : (\rho \mathbf{v} \mathbf{v}) + \nabla P_1 - \rho_1 \mathbf{g}_0 = 0 \quad (17)$$

$$\frac{\partial \rho_1}{\partial t} + \nabla \cdot (\rho \mathbf{v}) = 0. \quad (18)$$

where ω_{osc} is the mode frequency, P , ρ , \mathbf{v} and \mathbf{g} denote respectively the gas pressure, density, velocity and gravity.

The perturbed equation of state to second order in a Eulerian description is given by:

$$P_1 = c_s^2 \rho_1 + \alpha_s s_1 + \alpha_{\rho\rho} \rho_1^2 + \alpha_{ss} s_1^2 + \alpha_{\rho s} \rho_1 s_1 \quad (19)$$

where s is the entropy, $\alpha_s = (\partial P / \partial s)_\rho$, $c_s = \Gamma_1 P_0 / \rho_0$ denotes the average sound speed, $\Gamma_1 = (\partial \ln P / \partial \ln \rho)_s$ is the adiabatic exponent and $\alpha_{\rho\rho}$, α_{ss} and $\alpha_{\rho s}$ are the second partial derivatives of P versus s and ρ . Note that Eq. (19) assumes a constant chemical composition (this is indeed the case in the outer convective layers) but also constant ionisation rates.

The velocity field \mathbf{v} is split into a component due to the pulsational displacement $\delta \mathbf{r}_{\text{osc}}$ and a turbulent component \mathbf{u} as

$$\mathbf{v} = \mathbf{v}_{\text{osc}} + \mathbf{u} \quad (20)$$

Linearisation of Eq.(17-19) yields for the velocity field, in the absence of turbulence ($\mathbf{u} = 0$), the homogeneous wave equation

$$\left(\frac{\partial^2}{\partial t^2} - \mathbf{L} \right) \mathbf{v}_{\text{osc}} = 0 \quad (21)$$

where L is the linear wave operator (see its expression in SG). With appropriate boundary conditions (Unno et al. 1989) one recovers the usual eigenvalue problem :

$$\mathbf{L}(\boldsymbol{\xi}(\mathbf{r}, t)) = -\omega_{\text{osc}}^2 \boldsymbol{\xi}(\mathbf{r}, t) \quad (22)$$

where ω_{osc} is the mode eigenfrequency and $\boldsymbol{\xi}(\mathbf{r}, t) \equiv e^{-i\omega_{\text{osc}} t} \boldsymbol{\xi}(\mathbf{r})$ is the adiabatic displacement eigenvector.

In the presence of turbulence, the pulsational displacement ($\delta \mathbf{r}_{\text{osc}}$) is written in terms of the above adiabatic solution $\boldsymbol{\xi}(\mathbf{r}, t)$ and an instantaneous amplitude $A(t)$ according to Eq. (6). Under the assumption of a slowly varying intrinsic amplitude $A(t)$, the velocity (\mathbf{v}_{osc}) is related to $A(t)$ and $\delta \mathbf{r}_{\text{osc}}$ according to Eq. (7).

Differentiating Eq. (17) with respect to t , subtracting the time averaged equation of motion, neglecting non-linear terms in \mathbf{v}_{osc} , assuming an incompressible turbulence ($\nabla \cdot \mathbf{u} = 0$) and using Eqs. (18) and (19) yields the inhomogeneous wave equation

$$\rho_0 \left(\frac{\partial^2}{\partial t^2} - \mathbf{L} \right) [\mathbf{v}_{\text{osc}}] + \mathcal{D}[\mathbf{v}_{\text{osc}}] = \frac{\partial}{\partial t} \mathcal{S} - \mathcal{C} \quad (23)$$

with

$$\mathcal{S} \equiv \mathcal{S}_R + \mathcal{S}_S \quad (24)$$

$$\mathcal{S}_R = \nabla : (\rho_0 \mathbf{u} \mathbf{u}) - \nabla : (\langle \rho_0 \mathbf{u} \mathbf{u} \rangle) \quad (25)$$

$$\mathcal{S}_S = -\nabla (\bar{\alpha}_s s_t) \quad (26)$$

where s_t is the *Eulerian* turbulent entropy fluctuations and $\bar{\alpha}_s = \overline{(\partial P / \partial \rho)_s}$. The terms \mathcal{S}_R (Eq. (25)) and \mathcal{S}_S (Eq. (26)) are two driving sources, namely the Reynolds stress tensor and a term that involves the Eulerian entropy fluctuations. The last term \mathcal{C} in the RHS of Eq. (18) gathers terms that involve ρ_1 as well as the second order terms of Eq. (19). \mathcal{C} can in principle contribute to the driving. However, one can show that its contribution is negligible compared to \mathcal{S}_R and \mathcal{S}_S (see SG, GK).

The operator \mathcal{D} in the LHS of Eq. (18) involves both the turbulent velocity field (\mathbf{u}) and the pulsational velocity. This term contributes to the dynamical linear damping.

As we will see later, it is more convenient to decompose the Eulerian entropy fluctuations in terms of the Lagrangian ones, that is as:

$$\frac{\partial s_t}{\partial t} = \frac{d\delta s_t}{dt} - \mathbf{u} \cdot \nabla (s_0 + s_t) \quad (27)$$

where s_0 is the mean entropy. Accordingly, \mathcal{S}_S is such that:

$$\frac{\partial \mathcal{S}_S}{\partial t} = -\nabla \left(\frac{d}{dt} (\bar{\alpha}_s \delta s_t) - \bar{\alpha}_s \mathbf{u} \cdot \nabla s_t \right) \quad (28)$$

where we have dropped the term $\mathbf{u} \cdot \nabla s_0$ since it does not contribute to the driving (GK, see also SG). Integration of Eq. (28) with respect to time then gives \mathcal{S}_S .

4.2 General solution

Substituting Eq. (7) into Eq. (23), yields, with the help of Eq. (21), a differential equation for $A(t)$. This latter equation is straightforwardly solved and one obtains the solution for A :

$$A(t) = \frac{ie^{-\eta t}}{2\omega_{\text{osc}} I} \int_{-\infty}^t dt' \int_{\mathcal{V}} d^3x e^{(\eta + i\omega_{\text{osc}})t'} \boldsymbol{\xi}^*(\mathbf{x}) \cdot \mathcal{S}(\mathbf{x}, t') \quad (29)$$

where I is the mode inertia (which expression is given in Eq. (9)) and the spatial integration is performed over the stellar volume, \mathcal{V} . As the sources are random, A can only be calculated in square average, $\langle |A|^2 \rangle$. This statistical average is performed over a large set of realizations. From Eq. (29) and with the help of some simplifications as detailed in SG, one finds:

$$\langle |A|^2 \rangle = \frac{C^2}{8\eta(\omega_{\text{osc}} I)^2}, \quad (30)$$

with

$$C^2 \equiv \int_{\mathcal{V}} d^3x_0 \int_{-\infty}^{+\infty} d^3r d\tau e^{-i\omega_{\text{osc}}\tau} \langle \boldsymbol{\xi}^* \cdot \boldsymbol{\mathcal{S}}_1 \boldsymbol{\xi} \cdot \boldsymbol{\mathcal{S}}_2 \rangle \quad (31)$$

where η is the mode damping rate (which can be derived from seismic data), I the mode inertia (Eq. (9)), \mathbf{x}_0 the position in the star where the stochastic excitation is integrated, \mathcal{V} is the volume of the convective region, \mathcal{S} represents the different driving terms, \mathbf{r} , and τ are the spatial correlation and temporal correlation lengths associated with the local turbulence, subscripts 1 and 2 refer to quantities that are evaluated at the spatial and temporal positions $[\mathbf{x}_0 - \frac{\tau}{2}, -\frac{\tau}{2}]$ and $[\mathbf{x}_0 + \frac{\tau}{2}, \frac{\tau}{2}]$ respectively, and finally $\langle \cdot \rangle$ refers to a statistical average.

According to Eqs. (5), (8) and (30), the theoretical mode excitation rate, \mathcal{P} , is then given by the expression:

$$\mathcal{P} = \frac{C^2}{8I} \quad (32)$$

4.3 Driving sources

The Reynolds stress tensor (Eq. (25)) was identified early on by Lighthill (1952) as a source of acoustic noise and then as a source of *mode* excitation (GK). This term represents a mechanical source of driving and is considered by most of the theoretical formulations as the dominant contribution to the mode excitation (Goldreich & Keeley 1977b; Dolginov & Muslimov 1984; Balmforth 1992a; Stein & Nordlund 2001; Samadi et al. 2003a; Chaplin et al. 2005). However, as pointed-out by Osaki (1990), the first calculations by GK's significantly underestimate the power going to the solar modes compared to the observations.

In order to explain the mode excitation rates derived from the observations, Goldreich et al. (1994, GMK hereafter) identified the *Lagrangian* entropy fluctuations, i.e. the term δs_t in Eq. (28), as an additional driving source. These authors claimed that this term is the dominant source of driving. However, GMK assumed that entropy fluctuations (s_t) behave as a passive scalar. A passive scalar f is a quantity that obeys an equation of diffusion (see e.g. Lesieur 1997):

$$\frac{df}{dt} = \frac{\partial f}{\partial t} + \mathbf{u} \cdot \nabla f = \chi \nabla^2 f, \quad (33)$$

where χ is a diffusion coefficient. As shown by SG, assuming as GMK that δs_t is a passive scalar leads to a vanishing contribution. On the other hand, SG have shown that the term $\bar{\alpha}_s \mathbf{u} \cdot \nabla s_t$ in the RHS of Eq. (28) contributes effectively to the mode driving. In SG formulation, the so-called entropy source term is then :

$$\frac{\partial}{\partial t} \mathcal{S}_S = \nabla \cdot (\bar{\alpha}_s \mathbf{u} \cdot \nabla s_t). \quad (34)$$

The term $\mathbf{u} \cdot \nabla s_t$ in the RHS of Eq. (34) is an advective term. Since it involves the entropy fluctuations it can be considered as a thermal source of driving.

The source term of Eq. (34) was also identified by GK, but was considered as negligible. It must also be pointed out that the theoretical formalisms by Balmforth (1992a) and Chaplin et al. (2005) did not consider this source term. According to Samadi et al. (2003a), this term is not negligible (about $\sim 15\%$ of the total power) but nevertheless small compared to the Reynolds stress source term (\mathcal{S}_R) in the case of the Sun.

Finally, as seen in Eq. (31), \mathcal{S}_R and \mathcal{S}_S lead to cross terms. However, assuming as GMK that s_t behaves as a passive scalar and an *incompressible* turbulence (i.e. $\nabla \cdot \mathbf{u} = 0$), SG have shown that the crossing term between \mathcal{S}_R and \mathcal{S}_S vanishes. Hence, in the framework of those assumptions, there is *no canceling* between the two contributions (but see Sect. 8).

4.4 Length scale separation

As seen in the RHS of Eq. (31), the eigen-displacement $\boldsymbol{\xi}(\mathbf{r})$ is coupled spatially with the source function, \mathcal{S} . In order to derive a theoretical formulation that can be evaluated, it is necessary to spatially decouple $\boldsymbol{\xi}(\mathbf{r})$ from \mathcal{S} . This is the reason why all theoretical formulations explicitly or implicitly assume that eddies that effectively contribute to the driving have a characteristic length scale smaller than the mode wavelength. Indeed, provided this is the case, $\boldsymbol{\xi}(\mathbf{r})$ can be removed from the integral over r and τ that appears in the RHS of Eq. (30) (see SG). This assumption is justified for low turbulent Mach numbers M_t ($M_t \propto u/c_s$ where c_s is the sound speed). However, at the top of the solar convective zone, that is in the super-adiabatic region, M_t is no longer small ($M_t \sim 0.3$). Furthermore, for G and F stars lying on the main sequence, M_t is expected to increase with the effective temperature and to reach a maximum for $M \sim 1.6 M_\odot$ (see Houdek et al. 1999). Hence, for F type stars, significantly hotter than the Sun, the length scale separation becomes a more questionable approximation (see the discussion in Sect. 11).

4.5 Closure models

The second integral in RHS of Eq. (30) involves the term $\langle \mathcal{S}_1 \mathcal{S}_2 \rangle$, which is a two-point spatial *and* temporal correlation products of the source terms. Hence, the Reynolds stress source term (Eq. (25)) leads to the two-point correlation product of the form $\langle (\mathbf{u} \mathbf{u})_1 (\mathbf{u} \mathbf{u})_2 \rangle$. In the same way, the entropy source term (Eq. (34)) leads to the two-point correlation product of the form $\langle (\mathbf{u} s_t)_1 (\mathbf{u} s_t)_2 \rangle$. In both case, we deal with fourth-order two-point correlation product involving turbulent quantities (that is \mathbf{u} and s_t). Fourth-order moments are solutions of equations involving fifth-order moments. In turn, fifth-order moments are expressed in term of six-order moments ... and so on. This is the well known closure problem. A simple closure model is the quasi-normal approximation (QNA hereafter) that permits one to express fourth order moments in term of second order ones (see details in e.g. Lesieur 1997), that is :

$$\begin{aligned} \langle (u_i u_j)_1 (u_k u_l)_2 \rangle(\mathbf{r}, \tau) = & \langle (u_i u_j)_1 \rangle \langle (u_k u_l)_2 \rangle + \langle (u_i)_1 (u_l)_2 \rangle \langle (u_j)_1 (u_k)_2 \rangle \\ & + \langle (u_i)_1 (u_k)_2 \rangle \langle (u_j)_1 (u_l)_2 \rangle \end{aligned} \quad (35)$$

The decomposition of Eq. (35) is strictly valid when the velocity is normally distributed. The first term in the RHS of Eq. (35) cancels the term $\langle \mathbf{u} \mathbf{u} \rangle$ in Eq. (25) (see details in Chaplin et al. 2005). An expression similar to Eq. (35) is derived for the correlation product $\langle (\mathbf{u} s_t)_1 (\mathbf{u} s_t)_2 \rangle$ (see SG).

4.6 Adopted model of turbulence

It is usually more convenient to express Eq. (35) in the frequency (ω) and wavenumber (k) domains. We then define $\phi_{i,j}$ as the temporal and spatial Fourier transform of $\langle (u_i)_1 (u_j)_2 \rangle$. For an inhomogeneous, incompressible, isotropic and stationary turbulence, there is a relation between $\phi_{i,j}$ and the kinetic energy spectrum E , which is (Batchelor 1970):

$$\phi_{ij}(\mathbf{k}, \omega) = \frac{E(k, \omega)}{4\pi k^2} \left(\delta_{ij} - \frac{k_i k_j}{k^2} \right) \quad (36)$$

where k and ω are the wavenumber and frequency respectively associated with the turbulent elements, and $\delta_{i,j}$ is the Kronecker symbol. Following Stein (1967), it is possible to split for each layers $E(k, \omega)$ as:

$$E(k, \omega) = E(k) \chi_k(\omega) \quad (37)$$

where $E(k)$ is the time averaged kinetic energy spectrum and $\chi_k(\omega)$ is the frequency component of $E(k, \omega)$. In other words, $\chi_k(\omega)$ measures - in the frequency and k wavenumber domains - the temporal correlation between eddies. As discussed in Sect. 5.2, the way the eddy time-correlation is modeled has an important consequence on the efficiency of the mode driving. A decomposition similar to that of Eq. (37) is performed for the spectrum associated with the entropy fluctuations ($E_s(k, \omega)$).

Note that $\chi_k(\omega)$ and $E(k)$ satisfy by definition the following normalisation conditions:

$$\int_{-\infty}^{+\infty} d\omega \chi_k(\omega) = 1, \quad (38)$$

$$\int_0^{\infty} dk E(k) = \frac{1}{2} \langle \mathbf{u}^2 \rangle = \frac{\Phi}{2} \langle u_z^2 \rangle \equiv \frac{3}{2} u_0^2, \quad (39)$$

where u_z is the vertical component of the velocity, $\Phi \equiv \langle u^2 \rangle / \langle u_z^2 \rangle$ is the anisotropy factor introduced by Gough (1977), and u_0 is a characteristic velocity introduced for convenience. A normalisation condition similar to Eq. (39) is introduced for $E_s(k)$ (see details in SG).

4.7 Complete formulation

On the basis of the different assumptions mentioned above, SG then derive for *radial* modes the following theoretical expression for \mathcal{P} :

$$\mathcal{P} = \frac{1}{8I} (C_R^2 + C_S^2) \quad (40)$$

where C_R^2 and C_S^2 are the turbulent Reynolds stress and entropy contributions respectively. Their expressions are (see SG):

$$C_R^2 = 4 \pi^3 \mathcal{G} \int_0^M dm \rho_0 \left| \frac{d\xi_r}{dr} \right|^2 S_R(m, \omega_{\text{osc}}) \quad (41)$$

$$C_S^2 = \frac{4 \pi^3 \mathcal{H}}{\omega_{\text{osc}}^2} \int_0^M dm \frac{\bar{\alpha}_s^2}{\rho_0} g_r(\xi_r, m) S_S(m, \omega_{\text{osc}}) \quad (42)$$

with S_R and S_S are the source terms associated with the Reynolds stress and entropy fluctuations respectively:

$$S_R = \int_0^\infty dk \frac{E^2(k, m)}{k^2} \int_{-\infty}^{+\infty} d\omega \chi_k(\omega_{\text{osc}} + \omega, m) \chi_k(\omega, m) \quad (43)$$

$$S_S = \int_0^\infty dk \frac{E_s(k, m)E(k, m)}{k^2} \int_{-\infty}^{+\infty} d\omega \chi_k(\omega_{\text{osc}} + \omega, m) \chi_k(\omega, m) \quad (44)$$

In Eq. (41) and (42), ρ_0 is the mean density, \mathcal{G} and \mathcal{H} are two anisotropic factors (see their expressions in SG), and finally $g_r(\xi_r, m)$ is a function that involves the first and the second derivatives of ξ_r , its expression is:

$$g_r(\xi_r, m) = \left(\frac{1}{\alpha_s} \frac{d\alpha_s}{dr} \frac{d\xi_r}{dr} - \frac{d^2\xi_r}{dr^2} \right)^2 \quad (45)$$

It is in general more convenient to rewrite Eqs. (41) and (42) in the following forms:

$$C_R^2 = 4\pi^3 \mathcal{G} \int_0^M dm \frac{\rho_0 u_0^4}{k_0^3 \omega_0} \left| \frac{d\xi_r}{dr} \right|^2 \tilde{S}_R(m, \omega_{\text{osc}}), \quad (46)$$

$$C_S^2 = \frac{4\pi^3 \mathcal{H}}{\omega_{\text{osc}}^2} \int_0^M dm \frac{(\bar{\alpha}_s \tilde{s} u_0)^2}{\rho_0 k_0^3 \omega_0} g_r(\xi_r, m) \tilde{S}_s(m, \omega_{\text{osc}}) \quad (47)$$

where we have defined the dimensionless source functions $\tilde{S}_R \equiv (k_0^3 \omega_0 / u_0^4) S_R$ and $\tilde{S}_s \equiv (k_0^3 \omega_0 / (u_0^2 \tilde{s})) S_s$, \tilde{s} and where \tilde{s} is the rms of the entropy fluctuations. We have introduced for convenience the characteristic frequency ω_0 and the characteristic wavenumber k_0 ; they are defined as:

$$\omega_0 \equiv k_0 u_0 \quad (48)$$

$$k_0 \equiv \frac{2\pi}{\Lambda} \quad (49)$$

where Λ is a characteristic size derived from $E(k)$ and u_0 is the characteristic velocity given by Eq. (39). For future use, it is also convenient to define a characteristic time τ_0 as:

$$\tau_0 = \frac{2\pi}{k_0 u_0} = \frac{\Lambda}{u_0} \quad (50)$$

From Eq. (46) we can show that the driving by the Reynolds stress is locally proportional to the kinetic energy flux. Indeed, the flux of kinetic energy in the vertical direction is by definition:

$$F_{\text{kin}} \equiv w E_{\text{kin}} = w \left(\frac{1}{2} \rho_0 \mathbf{u}^2 \right) = \frac{3}{2} \sqrt{\frac{3}{\Phi}} \rho_0 u_0^3, \quad (51)$$

where $E_{\text{kin}} \equiv (1/2) \rho_0 \mathbf{u}^2$ is the kinetic energy per unit volume. Substituting Eq. (51) into Eq. (46) yields the relation:

$$C_R^2 \propto \int_0^M dm F_{\text{kin}} \Lambda^4 \left| \frac{d\xi_r}{dr} \right|^2 \tilde{S}_R(m, \omega_{\text{osc}}). \quad (52)$$

Concerning the driving by the entropy fluctuations, we can show that locally this driving does not only depend on F_{kin} but also on the convective flux (F_c). Indeed, let's define as GMK the quantity:

$$\mathcal{R} \equiv \frac{\alpha_s \tilde{s}}{\rho_0 u_0^2}. \quad (53)$$

Substituting Eq. (53) into Eq. (47) yields the relation:

$$C_S^2 \propto \int_0^M dm F_{\text{kin}} \Lambda^4 \mathcal{R}^2 \mathcal{F}^2 \left(\frac{\omega_0}{\omega_{\text{osc}}} \right)^2 \tilde{S}_S(m, \omega_{\text{osc}}), \quad (54)$$

where we have defined as in SG the quantity $\mathcal{F}^2 \equiv \Lambda^2 g_r$. Finally, since $\mathcal{R} \propto F_c/F_{\text{kin}}$ (see Samadi et al. 2006), we can conclude that locally the driving by entropy source term is proportional to F_{kin} and to the square of the ratio $\mathcal{R} \propto F_c/F_{\text{kin}}$.

5 Turbulent spectrum

As seen in Sect. 4.6, the model of stochastic excitation developed by SG involves $E(k, \omega)$, the turbulent kinetic spectrum as well as $E_s(k, \omega)$, the spectrum associated with the turbulent entropy fluctuations. Both spectra are split in terms of a time averaged spectrum ($E(k)$ for the velocity and $E_s(k)$ for the entropy fluctuations), and a frequency component $\chi_k(\omega)$ (see Sect. 4.6). Different prescriptions were investigated for both components. The results of these investigations are summarized in Sect. 5.1 for $E(k)$ and in Sect. 5.2 for $\chi_k(\omega)$.

5.1 Time averaged spectrum, $E(k)$

Two approaches are commonly adopted for prescribing $E(k)$. The classic one is to assume an analytical function derived either from theoretical considerations or empirical ones. The more commonly used analytical spectrum is the so-called Kolmogorov spectrum (Kolmogorov 1941), which derives originally from

Oboukhov (1941)’s postulate that energy is transferred from the large scales to the small scales at a constant rate. Other theoretical spectra, such as the so-called Spiegel’s spectrum (Spiegel 1962), or purely empirical spectra, such as those proposed by Musielak et al. (1994), were also considered. All of these analytical functions differ from each other by the way $E(k)$ varies with k . But for all of them, it is required to set a priori the characteristic wavenumber, k_0 , at which energy is injected into the turbulent cascade. The second approach consists to obtain $E(k)$ directly from hydrodynamical 3D simulations. This method has two advantages: it provides both the k dependence of $E(k)$ and the characteristic wavenumber k_0 . On the other hand, the inconvenient is that such method depends on the quality of the 3D hydrodynamical simulation.

These two approaches have been compared in Samadi et al. (2003b). Among the different analytical functions tested, the best agreement with a solar 3D simulation was found with the so-called “Extended Kolmogorov Spectrum” defined by Musielak et al. (1994). This spectrum increases at low scales as k^{+1} and decreases at low scales according to the Kolmogorov spectrum, i.e. as $k^{-5/3}$. However, due to the limited spatial resolution of the solar simulation used, the Kolmogorov scaling is validated over a limited range only. Nevertheless, the major part of the excitation arises from the most-energetic eddies, also referred to the energy bearing eddies. Accordingly, the contribution of the small scales, that are not resolved by the present 3D simulations, are expected to be relatively small. However, to confirm this, a quantitative estimate must be undertaken.

More important is the choice for the characteristic wavenumber k_0 . Indeed, the integrands of Eq. (46) and Eq. (47) are both proportional to k_0^{-4} . Accordingly, the computed \mathcal{P} are very sensitive to the choice for k_0 . This characteristic wavenumber can be obtained from 3D simulations. However, by default, one usually relates k_0 to the mixing-length Λ_{MLT} according to:

$$k_0 = k_0^{\text{MLT}} \equiv \frac{2\pi}{\beta \Lambda_{\text{MLT}}} \quad (55)$$

where $\Lambda_{\text{MLT}} = \alpha H_p$ is the mixing-length, α the mixing-length parameter, H_p the pressure scale height, and β a free parameter, which is usually set to a value of the order of one. The solar 3D simulation used by Samadi et al. (2003b) indicates that in the Sun $k_0 \simeq 3.6 \text{ Mm}^{-1}$ at the top of the excitation region. This characteristic wavenumber corresponds to an horizontal size of the granules of $\Lambda_g = 2\pi/k_0 \sim 2 \text{ Mm}$. This horizontal size is reached at the top of the excitation region with a value of β that depends on the adopted value for α and the solar 1D model used. For other stars, 3D simulations are rarely available. In that case, one usually assumes for β the same value that the one adopted for the Sun. Hence, an open and important question is whether or not the parameter β can be kept the same for other stars as for the Sun.

5.2 Eddy time-correlation, $\chi_k(\omega)$

Most of the theoretical formulations explicitly or implicitly assume a Gaussian function for $\chi_k(\omega)$ (Goldreich & Keeley 1977b; Dolginov & Muslimov 1984;

Goldreich et al. 1994; Balmforth 1992a; Samadi et al. 2001; Chaplin et al. 2005). However, 3D hydrodynamical simulations of the outer layers of the Sun show that, at the length associated with the energy bearing eddies, χ_k is rather Lorentzian (Samadi et al. 2003a). This is well illustrated in Fig. 3. As pointed-out by Chaplin et al. (2005), a Lorentzian χ_k is also a result predicted for the largest, most-energetic eddies by the time-dependent mixing-length formulation derived by Gough (1977). Therefore, there is some numerical and theoretical evidences that χ_k is rather Lorentzian at the length scale of the energy bearing eddies.

As shown by Samadi et al. (2003a), calculation of the mode excitation rates based on a Gaussian χ_k results for the Sun in a significant under-estimation of the maximum of \mathcal{P} whereas a better agreement with the observations is found when a Lorentzian χ_k is used. A similar conclusion is reached by Samadi et al. (2008) in the case of the star α Cen A. These results are illustrated in Fig. 5 in the case of the Sun and in Fig. 6 in the case of α Cen A.

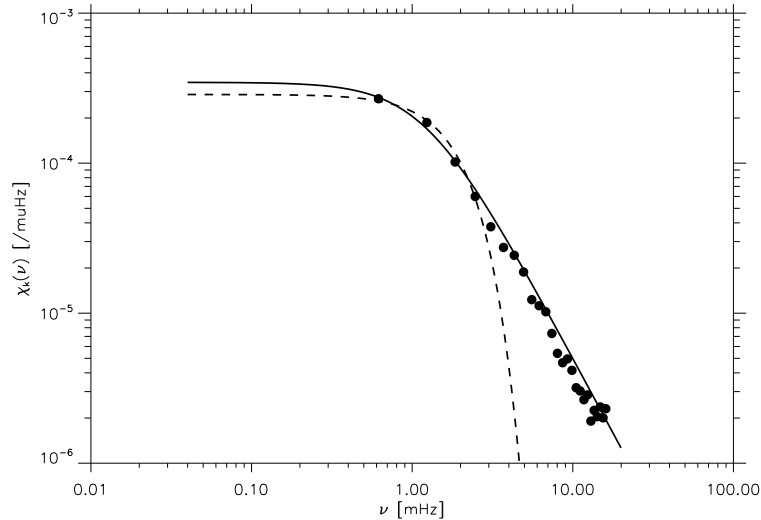


Fig. 3. Eddy time-correlation function, χ_k , as a function of frequency ν for the layer where the radial component of the velocity is maximum. The filled dots represent χ_k obtained from a solar 3D simulation with an horizontal resolution of $\simeq 25$ km (Samadi et al. 2003a). χ_k is shown here for the wavenumber k at which $E(k)$ peaks. The solid line represents a Lorentzian function and the dashed line a Gaussian function.

The excitation of low-frequency modes ($\nu \lesssim 3$ mHz) is mainly due to the large scale eddies. However, the higher the frequency the more important the contribution of the small scales. 3D solar simulations show that, at small scales, χ_k is neither Lorentzian nor Gaussian (Georgobiani et al. 2006). Hence, according to Georgobiani et al. (2006), it is impossible to separate the spatial component

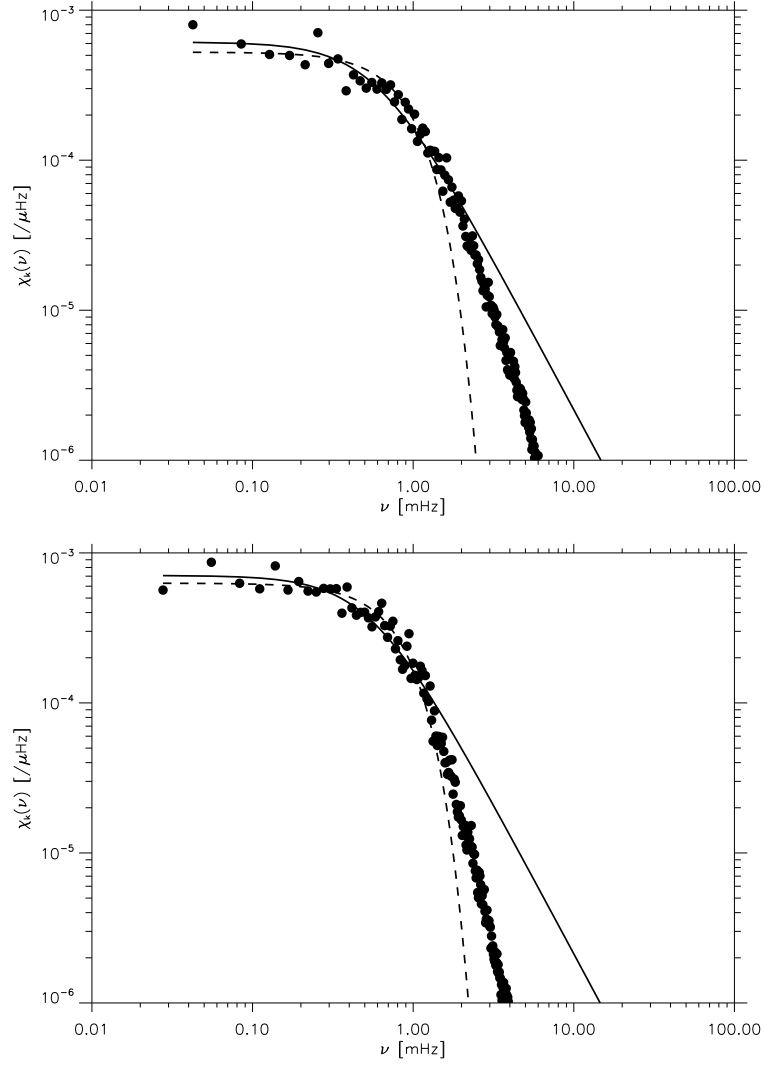


Fig. 4. **Top:** Same as Fig. 3 for a solar 3D simulation with an horizontal resolution of $\simeq 50$ km (Belkacem et al. 2006a). **Bottom:** Same as top for a solar 3D simulation with an horizontal resolution of $\simeq 120$ km.

$E(k)$ from the temporal component at all scales with the same simple analytical functions. However, such results are obtained using Large Eddy Simulation (LES). The way the small scales are treated in LES can affect our description of turbulence. Indeed, He et al. (2002) have shown that LES results in a $\chi_k(\omega)$ that decreases at all resolved scales too rapidly with ω with respect to direct numerical simulations (DNS). Moreover, Jacoutot et al. (2008b) found that computed mode excitation rates depend significantly on the adopted sub-grid model. Furthermore, Samadi et al. (2007) have shown that, at a given length scale, χ_k tends toward a Gaussian when the spatial resolution is decreased. This is illustrated in Fig. 4 by comparison with Fig. 3. In summary, the numerical resolution or the sub-grid model can substantially affect our description of the small scales. Improving the modeling of the excitation of the high frequency modes then requires more realistic and more resolved hydrodynamical 3D simulations.

Up to now, only analytical functions were assumed for $\chi_k(\omega)$. We have here implemented, for the calculation of \mathcal{P} , the eddy time-correlation function derived *directly* from long time series of 3D simulation realizations with an intermediate horizontal resolution ($\simeq 50$ km). As shown in Figs. 5 and 6, the mode excitation rates, \mathcal{P} , obtained from χ_k^{3D} , are found to be comparable to that obtained assuming a Lorentzian χ_k , except at high frequency in the case of the Sun. This is obviously the direct consequence of the fact that a Lorentzian χ_k reproduces rather well χ_k^{3D} (see Fig. 3), except at high frequency where χ_k^{3D} decreases more rapidly than the Lorentzian function (see Fig. 4 left). At high frequency, calculations based on a Lorentzian χ_k result in larger \mathcal{P} and reproduce better the helioseismic constraints than those based on χ_k^{3D} (see Fig. 5). This indicates perhaps that χ_k^{3D} decreases more rapidly with frequency than it should. This is consistent with He et al. (2002)'s results who found that LES predict a too rapid decrease with ν compared to the DNS (see above).

Chaplin et al. (2005) also found that the use of a Gaussian χ_k severely underestimates the observed solar mode excitation rates. However, in contrast with Samadi et al. (2003a), they mention that a Lorentzian χ_k results in a severe over-estimation for the low-frequency modes. In order to illustrate the results by Chaplin et al. (2005), we have computed the solar mode excitation rates using their formalism and a solar envelope equilibrium model similar to the one considered by these authors (see Samadi et al. 2003b). The result is shown in Fig. 7. We clearly see that the mode excitation rates computed using a Gaussian χ_k overestimate by ~ 20 the seismic constraints. This result is consistent with this found by Samadi et al. (2003a). On the other hand, in contrast with Samadi et al. (2003a), the modes with frequency below $\nu \sim 2$ mHz are severely over-estimated when a Lorentzian χ_k is assumed. It should be pointed out that the excitation of modes with frequency $\nu \lesssim 2$ mHz occurs in a region more extended than covered by the solar 3D simulation used by Samadi et al. (2003b). On the other hand, the pure 1D modeling by Chaplin et al. (2005), includes all of the convective zone. The severe over-estimation at low frequency of the mode excitation rates, is explained by the authors by the fact that, at a given frequency, a Lorentzian χ_k decreases too slowly with depth compared to a Gaus-

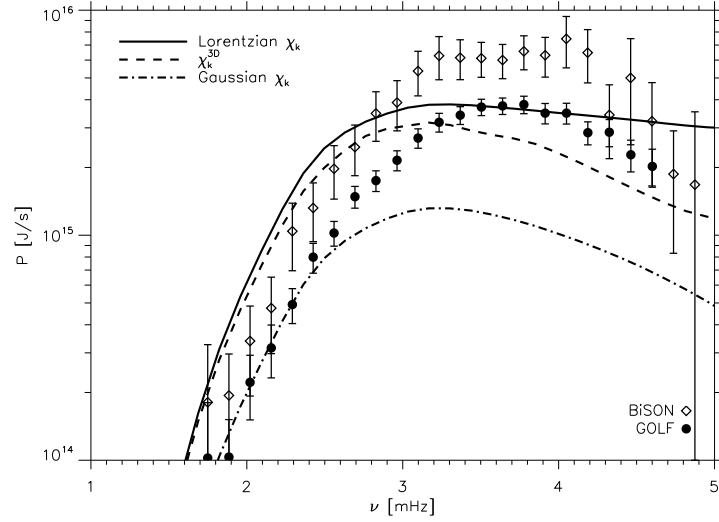


Fig. 5. Solar p -mode excitation rates as a function of ν . Filled circles and diamonds correspond as in Fig. 1 to seismic data from SOHO/GOLF and BiSON network respectively. The lines correspond to semi-theoretical calculations based on different choices for χ_k : Lorentzian χ_k (solid line), χ_k^{3D} i.e. χ_k derived directly from the solar 3D simulation (dashed line), and a Gaussian χ_k (dot-dashed line).

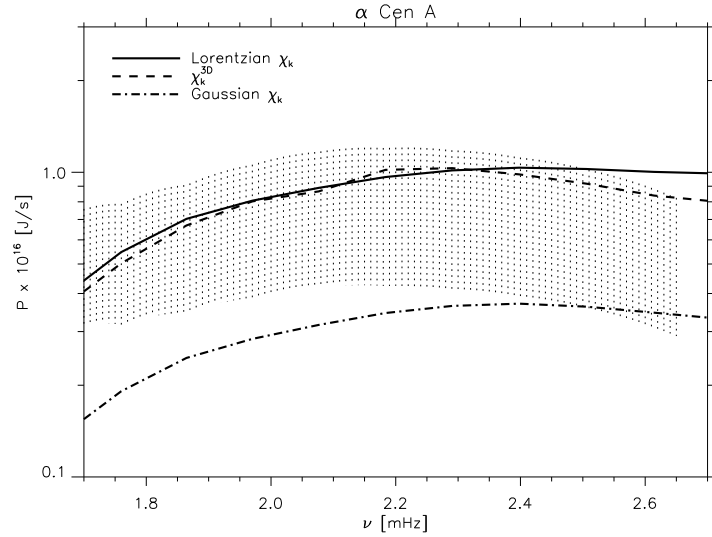


Fig. 6. Same as in Fig. 5 for the case of α Cen A.

sian χ_k . Consequently, for the low-frequency modes, a substantial fraction of the integrand of Eq. (41) arises from large eddies situated deep in the Sun. This might suggest that, in the deep layers, the eddies that contribute efficiently have rather a Gaussian χ_k . However, this remains an open issue.

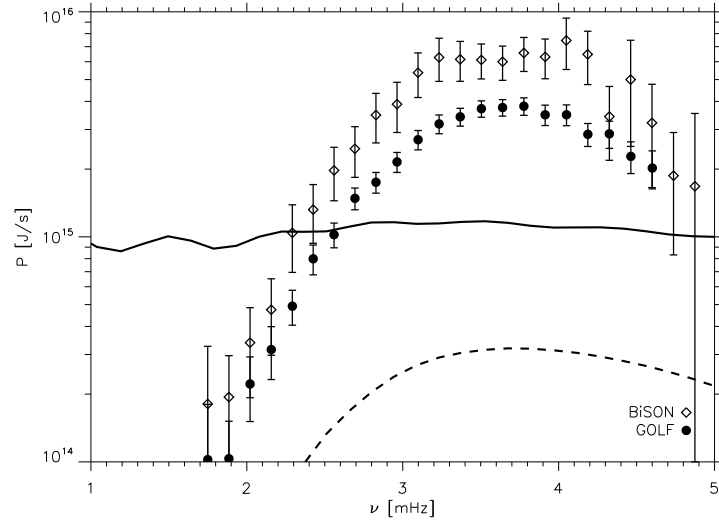


Fig. 7. Same as Fig. 5. The lines correspond to calculations using the formalism by Chaplin et al. (2005). Two choices for χ_k was considered : a Lorentzian χ_k (solid line) and a Gaussian χ_k (dashed line). In both calculations, driving due to the entropy fluctuations is not included.

6 Closure models and anisotropy

The decomposition of Eq. (35) assumes the quasi-normal approximation (QNA). However, it is well known that the departure from the QNA is important in a strongly turbulent medium. In addition, a closure model based on the QNA does not ensure the positiveness of the energy (see details in e.g. Lesieur 1997). Furthermore, the QNA is strictly valid only for normally distributed fluctuating quantities with zero mean. However, the upper-most part of the convection zone is a turbulent convective medium composed of essentially two flows that are asymmetric with respect to each other. Hence, in such a medium, the probability distribution function of the fluctuations of the vertical velocity and temperature do not follow a Gaussian law. As verified by Belkacem et al. (2006a, B06a hereafter) and Kupka & Robinson (2007), departure from the QNA is important in the upper part of the solar convective zone. Indeed, this approximation underestimates, in the quasi-adiabatic region, by $\approx 50\%$ the fourth-order moment of the vertical velocity derived from a solar 3D simulation.

The term in the LHS of Eq. (35) corresponds to a two-point correlation product involving the velocity, i.e. $\langle (u_i u_j)_1 (u_k u_l)_2 \rangle(r, \tau)$ where r and τ are the spatial correlation and temporal correlation lengths respectively. For $r \rightarrow 0$ and $\tau \rightarrow 0$, this term reduces to a *one-point* correlation product, $\langle u_i u_j u_k u_l \rangle$, also referred as a fourth-order moment (FOM hereafter). As we shall see below, it is possible to derive an improved closure model for this term that does not rely on the QNA. However, we still require a prescription for the *two point* correlation products involving the velocity ($\langle (u_i u_j)_1 (u_k u_l)_2 \rangle(r, \tau)$) and the entropy fluctuations ($\langle (\mathbf{u} s_t)_1 (\mathbf{u} s_t)_2 \rangle(r, \tau)$). For radial modes or low ℓ order modes, only the radial component of the velocity (w) matters. Hence, for these modes we require a prescription for $\langle w_1^2 w_2^2 \rangle(r, \tau)$ and $\langle (w s_t)_1 (w s_t)_2 \rangle(r, \tau)$. By default, Belkacem et al. (2006b) have proposed that $\langle w_1^2 w_2^2 \rangle(r, \tau)$ varies with r and τ in the same way than in the QNA (Eq. (35)), that is:

$$\langle w_1^2 w_2^2 \rangle = \frac{\mathcal{K}_w}{3} \langle w_1^2 w_2^2 \rangle_{\text{QNA}}, \quad (56)$$

where \mathcal{K}_w is a constant and $\langle w_1^2 w_2^2 \rangle_{\text{QNA}}$ is the two-point correlation product given for w according to the QNA (Eq. (35)). Accordingly, the contribution of the Reynolds stress (C_R^2 , Eq. (41)) is modified as:

$$C_R^2 = 4 \pi^3 \mathcal{G} \int_0^M dm \rho_0 \left(\frac{d\xi_r}{dr} \right)^2 \frac{\mathcal{K}_w}{3} S_R(m, \omega_{\text{osc}}) \quad (57)$$

Note that the contribution of the entropy fluctuations (C_S^2 , Eq. (42)) still assumes the QNA. This inconsistency has a small impact on computed mode excitation rates since C_S^2 is significantly smaller than C_R^2 , at least for stars that are not too hot (but see Sect. 8).

The constant \mathcal{K}_w is determined in the limit case where $r \rightarrow 0$ and $\tau \rightarrow 0$. Indeed, when $r \rightarrow 0$ and $\tau \rightarrow 0$, we have:

$$\langle w^4 \rangle = \frac{\mathcal{K}_w}{3} \langle w^4 \rangle_{\text{QNA}}, \quad (58)$$

where $\langle w^4 \rangle$ is by definition the fourth-order moment (FOM hereafter) associated with w and $\langle w^4 \rangle_{\text{QNA}}$ is the one given by the QNA. In the same way, Eq. (35) gives :

$$\langle w^4 \rangle_{\text{QNA}} = 3 \langle w^2 \rangle^2. \quad (59)$$

Using Eqs. (58) and (59), we then derive the constant \mathcal{K}_w :

$$\mathcal{K}_w = 3 \frac{\langle w^4 \rangle}{\langle w^4 \rangle_{\text{QNA}}} = \frac{\langle w^4 \rangle}{\langle w^2 \rangle^2}, \quad (60)$$

which is by definition the Kurtosis. This quantity measures the oblateness of the probability density function (see e.g. B06a). For normally distributed w we have $\mathcal{K}_w = 3$. The Kurtosis then measures the departure of the FOM from the QNA.

Closure models more sophisticated than the QNA can be used. Among those, the two-scale mass flux model (Abdella & McFarlane 1997) improved by Gryanik & Hartmann (2002) takes the asymmetries in the medium into account but is only applicable for quasi-laminar flows. For \mathcal{K}_w , Gryanik & Hartmann (2002) obtained the following expression:

$$\mathcal{K}_w = (1 + S_w^2) \quad (61)$$

with the skewness, S_w , given by:

$$S_w \equiv \frac{\langle w^3 \rangle}{\langle w \rangle^{3/2}} = \frac{1 - 2a}{\sqrt{a(1 - a)}} \quad (62)$$

where a is the mean fractional area occupied by the updrafts in the horizontal plane. In the QNA limit, i.e. when the random quantities are distributed according to a Normal distribution with zero mean, we necessarily have $S_w = 0$. Hence, in the QNA limit, Eq. (61) does not match the expected value i.e. $\mathcal{K}_w = 3$. Then, Gryanik & Hartmann (2002) proposed to modify Eq. (61) as follows:

$$\mathcal{K}_w = 3 \left(1 + \frac{1}{3} S_w^2 \right). \quad (63)$$

Figure 8 shows that the FOM based on Eq. (63) with S_w given by Eq. (62), results in a negligible improvement with respect to the QNA. However, when S_w is derived directly from the 3D simulation and plugged into Eq. (63), Eq. (63) is then a very good evaluation of the FOM derived from a 3D simulation of the outer layer of the Sun as verified by B06a and Kupka & Robinson (2007).

Belkacem et al. (2006a) have generalized Gryanik & Hartmann (2002)'s approach by taking the skewness introduced by the presence of up- and down-drafts *and* the turbulent properties of each flow into account. Accordingly, they have derived a more accurate expression for S_w (see the expression in B06a). As shown in Fig. 8, calculations of the FOM based on Eq. (63) and their expression for S_w reproduce rather well – in the quasi-adiabatic region – the FOM derived from the solar 3D simulation.

Belkacem et al. (2006b) have computed mode excitation rates, \mathcal{P} according to Eq. (57) with the Kurtosis \mathcal{K}_w given by Eq. (63) and with the skewness S_w computed according to B06a's closure model. The maximum in \mathcal{P} is found about 30% larger than in calculations based on the QNA and fits better the maximum in \mathcal{P} derived from the helioseismic data. This increase is significantly larger than the entropy contribution (the term \mathcal{S}_S in Eq. (42), which is of the order of $\sim 15\%$, see Sect. 8). We stress that, however, 30% is of the same order as the difference between seismic constraints of different origins (SOHO/GOLF, GONG, BiSON). These results are illustrated in Fig. 9.

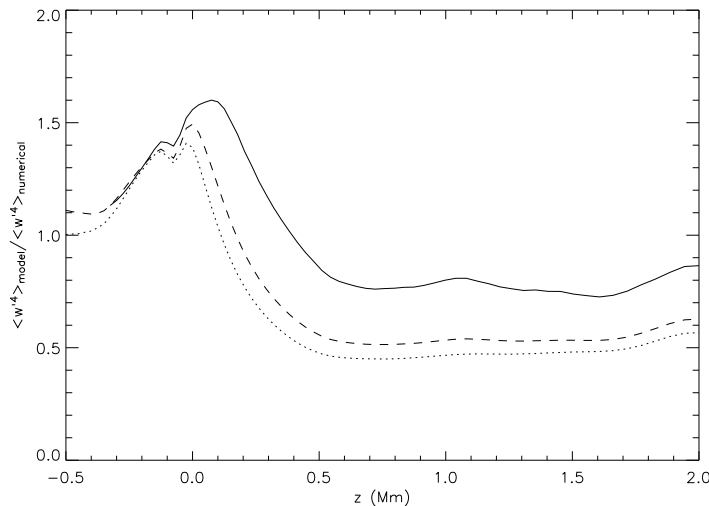


Fig. 8. Fourth-order moment (FOM) of the velocity, $\langle w^4 \rangle = \mathcal{K}_w \langle w^2 \rangle^2$, as a function of depth z , normalized to the FOM derived from the 3D simulation. In all cases the Kurtosis \mathcal{K}_w , (Eq. (60)) is calculated according to Eq. (63) but with different skewness, S_w . The solid line S_w is computed according to B06a’s closure model, the dashed line assumes Gryanik & Hartmann (2002)’s expression for S_w (Eq. (62)) and finally the dotted line assumes the QNA, that is $S_w = 0$ and $\mathcal{K}_w = 3$.

7 Importance of the stellar stratification and chemical composition

7.1 Role of the turbulent pressure

Rosenthal et al. (1999) have shown that taking the turbulent pressure into account in a realistic way in the 1D global solar models results in a much better agreement between observed and theoretical mode frequencies of the Sun. Following Rosenthal et al. (1999), Samadi et al. (2008) have studied the importance for the calculation of the mode excitation rates of taking the turbulent pressure into account in the averaged 1D model. For this purpose, they have built two 1D models representative of the star α Cen A. One model (here referred as the “patched” model), has its surface layers taken directly from a fully compressible 3D hydrodynamical numerical model. A second model (here referred as “standard” model), has its surface layers computed using standard physics, in particular convection is described according Böhm-Vitense (1958)’s mixing-length local theory of convection (MLT) and turbulent pressure is ignored.

Samadi et al. (2008) found that the calculations of \mathcal{P} involving eigenfunctions computed on the basis of the “patched” global 1D model reproduce much better the seismic data derived for α Cen A than calculations based on the eigenfunctions computed with the “standard” stellar model, i.e. built with the MLT

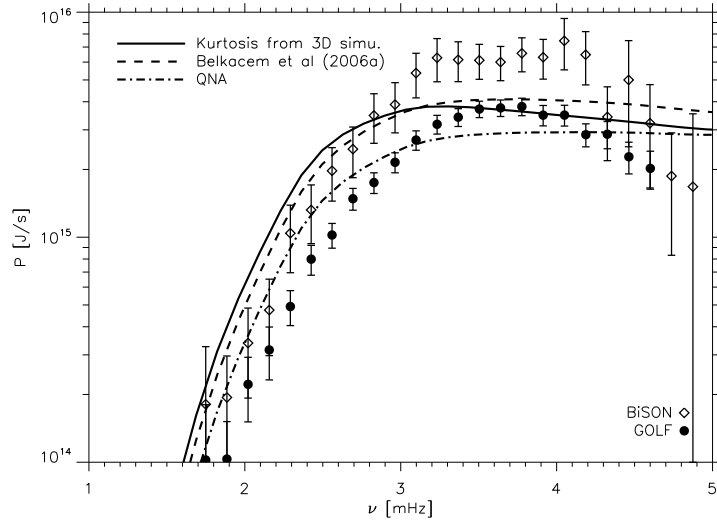


Fig. 9. Same as in Fig. 5. The thick lines correspond to calculations where the Reynolds stress contribution is computed according to Eq. (57). The Kurtosis (K_w) is computed here in a different manner: for the solid line K_w is obtained directly from a 3D solar simulation, for the dashed line the Kurtosis is calculated according to Eq. (63) where the skewness (S_w) is obtained from B06a’s closure model, and finally for the dot-dashed line we have assumed the QNA, that is $S_w = 0$ and $K_w = 3$.

and ignoring turbulent pressure. This is because a model that includes turbulent pressure results in *lower* mode masses \mathcal{M} than a model that ignores turbulent pressure. This can be understood as follows: Within the super-adiabatic region, a model that includes turbulent pressure provides an additional support against gravity, hence has a lower gas pressure and density than a model that does not include turbulent pressure (see also Nordlund & Stein 1999; Rosenthal et al. 1999). As a consequence, mode inertia (Eq. (9)) or equivalently mode masses (Eq. (11)) are then *lower* in a model that includes turbulent pressure.

7.2 Role of the surface metal abundance

Samadi et al. (2009c) have recently studied the role of the surface metal abundance on the efficiency of the stochastic driving. For this purpose, they have computed two 3D hydrodynamical simulations representative – in effective temperature and gravity – of the surface layers of HD 49933, a star which is rather metal poor compared to the Sun since its surface iron-to-hydrogen abundance is $[\text{Fe}/\text{H}] = -0.37$. One 3D simulation (hereafter labeled as S0) has a solar metal abundance and the other (hereafter labeled as S1) has $[\text{Fe}/\text{H}]$ ten times smaller. For each 3D simulation they have build a “patched” model in the manner of Samadi et al. (2008) and computed the acoustic modes associated with the “patched” model.

As seen in Fig. 10, the mode excitation rates \mathcal{P} associated with S1 are found to be about *three times smaller* than those associated with S0. This difference is related to the fact that a lower surface metallicity results in a lower opacity, and accordingly in an higher surface density. In turn, the higher the density, the smaller are the convective velocities to transport by convection the same amount of energy. Finally, smaller convective velocities result in a less efficient driving (for details see Samadi et al. 2009c). This conclusion is qualitatively consistent with that by Houdek et al. (1999) who – on the basis of a mixing-length approach – also found that the mode amplitudes decrease with decreasing metal abundance.

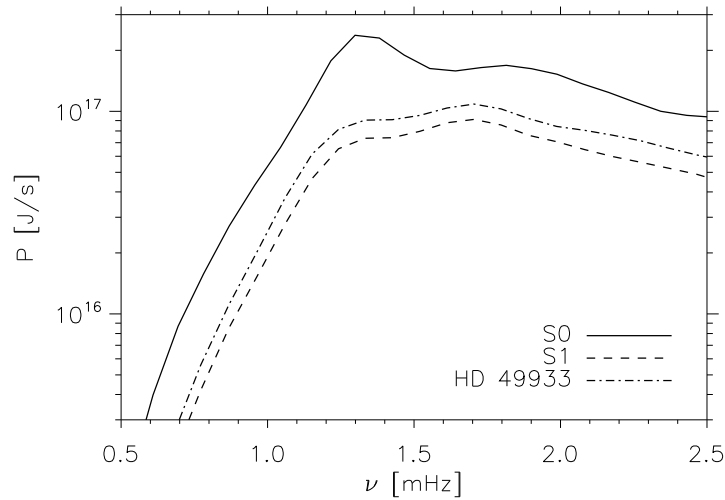


Fig. 10. Mode excitation rates, \mathcal{P} , as a function of the mode frequency (ν) obtained for two 3D models with the effective temperature and the surface gravity of HD 49933 but with two different surface metal abundances (see Sect. 7.2 and Samadi et al. (2009c)). The solid line corresponds to the 3D model with the metal abundance (S0) and the dashed line to metal poor 3D model (S1). The dot-dashed line corresponds to the mode excitation rates derived for the specific case of HD 49933 as explained in Samadi et al. (2009c).

Using the seismic determinations of the mode linewidths measured by CoRoT for HD 49933 (Benomar et al. 2009) and the theoretical mode excitation rates computed for the specific case of HD 49933, Samadi et al. (2009b) have derived the theoretical mode amplitudes of the acoustic modes of HD 49933. Except at rather high frequency ($\nu \gtrsim 1.9$ mHz), their amplitude calculations are within approximately $1\text{-}\sigma$ in agreement with the mode amplitudes derived from the CoRoT data (for more details see Samadi et al. 2009b). They also show that assuming a solar metal abundance rather than the observed metal abundance of the star would result in larger mode amplitudes and hence in a larger discrepancy

with the seismic data. This illustrates the importance of taking the surface metal abundance of the solar-like pulsators into account when modeling the mode excitation.

8 Contribution of the entropy fluctuations

Using the method summarised in Sect. 9.2, Stein & Nordlund (2001) have computed *directly* from a 3D simulation of the surface of the Sun the contribution of the incoherent entropy fluctuations (Eq. (26)). They also found that the entropy fluctuation is small compared to the Reynolds stress contribution. However, as shown by Samadi et al. (2007), the relative contribution of the entropy to the total excitation rate increases rapidly with the effective temperature, T_{eff} . For instance, the solar-like pulsator HD 49333 has a significantly higher T_{eff} than the Sun. Samadi et al. (2009c) found that for this star the entropy fluctuations contributes up to $\sim 30\%$ while it is only about 15% in the case of the Sun (see Samadi et al. 2007) and in the case of α Cen A (see Samadi et al. 2008).

As pointed-out by Houdek (2006), the solar and stellar 3D simulations performed by Stein et al. (2004) show some partial canceling between the Reynolds stress contribution (\mathcal{S}_R , Eq. (25)) and contribution due to the entropy (\mathcal{S}_S , Eq. (26)). This cancellation increases with increasing T_{eff} (see Stein et al. 2004). In the theoretical model of stochastic excitation, the cross terms between the entropy fluctuations and the Reynolds stresses vanish (see Sect. 4.3). As originally suggested by Houdek (2006) and discussed in Samadi et al. (2009b), the existence of a partial canceling can decrease the mode amplitude and improve the agreement with the seismic observations. However, there is currently no theoretical modeling of the interference between these two terms (see the discussion in Sect. 11 and in Samadi et al. (2009b)).

9 Alternative approaches

9.1 Energy equipartition

Under certain conditions that we will emphasize below, GK have shown that there is an equipartition of kinetic energy between an acoustic mode and the resonant eddy. To derive this principle, GK assume that the acoustic modes are damped by turbulent viscosity *and* excited by the Reynolds stresses. We reproduce here their demonstration. For the sake of simplicity, we will consider modes with $\omega_{\text{osc}} \tau_0 \lesssim 1$ where τ_0 is the characteristic time of the energy bearing eddies typically located in the upper part of the convective zone, that is the region where the driving is the most vigorous. Furthermore, we neglect as did GK the driving by the entropy fluctuations (Eq. (42)). According to Eqs. (40) and (52), we have roughly for acoustic modes with $\omega_{\text{osc}} \tau_0 \lesssim 1$:

$$\mathcal{P} \propto \frac{1}{I} \int dm \left| \frac{d\xi_r}{dr} \right|^2 E_{\text{eddy}} \Lambda u_0, \quad (64)$$

where Λ is the characteristic size of the energy bearing eddies, u_0 their characteristic velocity (Eq. (39)), $\tau_0 = \Lambda/u_0$ their characteristic lifetime (Eq. (50)), and $E_{\text{eddy}} = (3/2) \rho_0 u_0^2 \Lambda^3$ their total kinetic energy. Let k_{osc} be the vertical oscillation wave number. We have then $d\xi_r/dr = i k_{\text{osc}} \xi_r$. We further assume that – in the driving region – the acoustic waves are purely propagating. This assumption then implies $\omega_{\text{osc}} = k_{\text{osc}} c_s$ where c_s is the sound speed. Accordingly, we can simplified Eq. (64) as:

$$\mathcal{P} \propto \frac{\omega_{\text{osc}}^2}{I} \int dm \left(\frac{\xi_r}{c_s} \right)^2 E_{\text{eddy}} \Lambda u_0 . \quad (65)$$

In the region where the mode are excited, E_{eddy} , u_0 , and c_s vary quite rapidly. However, again for the sake of simplicity we will assume that these quantities are constant and evaluate them at the layer where the excitation is the most efficient, i.e. at the peak of the super-adiabatic temperature gradient. The integration of Eq. (64) can be approximated as

$$\mathcal{P} \propto \frac{1}{I} \left(\frac{\omega_{\text{osc}}}{c_s} \right)^2 E_{\text{eddy}} \Lambda u_0 \int dm \xi_r^2 . \quad (66)$$

Using the expression of the mode inertia (Eq. (9)), we can finally simplify Eq. (66) as:

$$\mathcal{P} \propto \left(\frac{\omega_{\text{osc}}}{c_s} \right)^2 E_{\text{eddy}} \Lambda u_0 . \quad (67)$$

Modes damped by turbulent viscosity have their damping rates η given by (Ledoux & Walraven 1958; Goldreich & Keeley 1977a),

$$\eta \propto \frac{1}{3I} \int dm \nu_t \left| r \frac{d}{dr} \left(\frac{\xi_r}{r} \right) \right|^2 , \quad (68)$$

where ν_t is the turbulent viscosity. The simplest prescription for ν_t is the concept of eddy-viscosity. This consists in assuming $\nu_t = u_0 \lambda = \tau_0 u_0^2$. Obviously the turbulent medium is characterized by eddies with a large spectrum of size. However, only the eddies for which $\omega_{\text{osc}} \tau_\lambda \approx 1$ are expected to efficiently damp the mode with frequency ω_{osc} . Since we are looking at the modes such that $\omega_{\text{osc}} \tau_\lambda \lesssim 1$, only the largest eddies efficiently damp the mode, that is the eddies with size Λ . Accordingly, we adopt $\nu_t = u_0 \Lambda$. With the same simplifications and assumptions as those used for deriving Eq. (67), we can simplify Eq. (68) as:

$$\eta \propto \left(\frac{\omega_{\text{osc}}}{c_s} \right)^2 \Lambda u_0 . \quad (69)$$

From Eqs. (5), (67) and (69), we then derive the mode kinetic energy:

$$E_{\text{osc}} \propto E_{\text{eddy}} . \quad (70)$$

Eq. (70) highlights an equipartition of kinetic energy between an acoustic mode and the resonant eddies. Christensen-Dalsgaard & Frandsen (1983) used this “equipartition principle” to derive the first quantitative estimate of solar-like oscillations in stars. The relation of Eq. (70) was derived by assuming that modes are damped by turbulent viscosity. However, as pointed-out by Osaki (1990), theoretical mode line-widths, $\Gamma = \eta/\pi$, computed in the manner of Goldreich & Keeley (1977a), i.e. assuming a viscous damping, are underestimated compared to the observations. Gough (1976) proposed a different prescription for ν_t . Nevertheless, assuming Gough (1976)’s prescription also results in similar Γ (see Balmforth 1992b). On the other hand, Xiong et al. (2000) report that the turbulent viscosity is the dominant source of damping of the radial p modes. As discussed recently by Houdek (2008), there is currently no consensus about the physical processes that contribute dominantly to the damping of p modes. If the damping due to turbulent viscosity turns out to be negligible, then there is no reason that the balance between the mode kinetic energy and the kinetic energy of resonant eddies holds in general.

9.2 “Direct” calculation

The model of stochastic excitation presented in Sect. 4 is based on several simplifications and assumptions concerning the turbulence and the source terms. There is an alternative approach proposed by Nordlund & Stein (2001) that does not rely on such simplifications and assumptions. In such approach, the rate at which energy is stochastically injected into the acoustic modes is obtained *directly* from 3D simulations of the outer layers of a star by computing the (incoherent) work performed on the acoustic mode by turbulent convection. In their approach, the energy input per unit time into a given acoustic mode is calculated numerically according to Eq. (74) of Nordlund & Stein (2001) multiplied by S , the area of the simulation box, to get the excitation rate (in J s^{-1}):

$$\mathcal{P}_{3\text{D}}(\omega_{\text{osc}}) = \frac{\omega_{\text{osc}}^2 S}{8 \Delta\nu \mathcal{E}_{\omega_{\text{osc}}}} \left| \int_r dr \Delta\hat{P}_{\text{nad}}(r, \omega_{\text{osc}}) \frac{\partial \xi_r}{\partial r} \right|^2 \quad (71)$$

where $\Delta\hat{P}_{\text{nad}}(r, \omega)$ is the discrete Fourier component of the non-adiabatic pressure fluctuations, $\Delta P_{\text{nad}}(r, t)$, estimated at the mode eigenfrequency $\omega_{\text{osc}} = 2\pi\nu_0$, ξ_r is the radial component of the mode displacement eigenfunction, $\Delta\nu = 1/T_s$ the frequency resolution corresponding to the total simulation time T_s and $\mathcal{E}_{\omega_{\text{osc}}}$ is the normalised mode energy per unit surface area defined in Nordlund & Stein (2001, their Eq. (63)) as:

$$\mathcal{E}_{\omega_{\text{osc}}} = \frac{1}{2} \omega_{\text{osc}}^2 \int_r dr \xi_r^2 \rho \left(\frac{r}{R} \right)^2. \quad (72)$$

Eq. (71) corresponds to the calculation of the PdV work associated with the non-adiabatic gas and turbulent pressure (Reynolds stress) fluctuations. In contrast to the pure theoretical models (see Sect. 4), the derivation of Eq. (71)

does not rely on a simplified model of turbulence. For instance, the relation of Eq. (36) is no longer required. Furthermore, they do not assume that entropy fluctuations behave as a passive scalar (Eq. (33)). However, as for the theoretical models, it is assumed that ξ_r varies on a scale-length larger than the eddies that contributes effectively to the driving (this is the so-called “length-scale separation”, see Sect. 4.4). In addition, Eq. (71) implicitly assumes the quasi-Normal approximation (Eq. (35)).

The expression of Eq. (71) has been applied to the case of the Sun by Stein & Nordlund (2001). These authors obtain a rather good agreement between \mathcal{P}_{3D} (Eq. (71)) and the solar mode excitation rates derived from the GOLF instrument by Roca Cortés et al. (1999). However, solar mode excitation rates derived by Stein & Nordlund (2001) from the seismic analysis by Roca Cortés et al. (1999) are – for a reason that remains to be understood – systematically lower than those derived from the seismic analysis by Baudin et al. (2005). Stein et al. (2004) have computed \mathcal{P}_{3D} (Eq. 71) for a set of stars located near the main sequence from K to F and a subgiant K IV star. The comparison between these calculations and those based on SG’s formalism has been undertaken by Samadi et al. (2007). The maximum in \mathcal{P}_{3D} was found systematically lower than those from calculations based on SG’s formalism (Eqs. (40)-(44)). These systematic differences were attributed by Samadi et al. (2007) to the low spatial resolution of the hydrodynamical 3D simulations computed by Stein et al. (2004).

10 Stochastic excitation across the HR diagram

10.1 Mode excitation rates

Using several 3D simulations of the surface of main sequence stars, Samadi et al. (2007) have shown that the maximum of the mode excitation rates, \mathcal{P}_{\max} , varies with the ratio L/M as $(L/M)^\alpha$ where L and M are the luminosity and the mass of the star respectively and α is the slope of this scaling law. Furthermore, they found that the slope α is rather sensitive to the adopted function for χ_k : $\alpha=3.1$ for a Gaussian χ_k and $\alpha=2.6$ for a Lorentzian one.

The increase of \mathcal{P}_{\max} with L/M is not surprising: It should first be noticed that, even though the ratio L/M is the ratio of two global stellar quantities, it nevertheless essentially characterizes the properties of the stellar surface layers where the mode excitation is located since $L/M \propto T_{\text{eff}}^4/g$. Indeed, by definition of the effective temperature, T_{eff} , and the stellar radius R , the total luminosity of the star, L , is given by the Steffan’s law: $L = 4\pi\sigma T_{\text{eff}}^4 R^2$ where σ is Stefan’s constant. Furthermore, the surface gravity is $g = GM/R^2$ where G is the gravitational constant. Accordingly, $L/M \propto T_{\text{eff}}^4/g$.

Second, as we will show now, it is possible to roughly explain the dependence of \mathcal{P}_{\max} with g and T_{eff}^4 . Eq. (67) can be rewritten as:

$$\mathcal{P} \propto \left(\frac{\omega_{\text{osc}}}{c_s} \right)^2 F_{\text{kin}} A^4. \quad (73)$$

where

$$F_{\text{kin}} = \frac{3}{2} \rho_0 u_0^3 \quad (74)$$

is by definition the flux of kinetic energy per unit volume⁵ and u_0 is the characteristic velocity given by Eq. (39).

The characteristic size Λ is approximately proportional to the pressure scale height H_p (see e.g. Samadi et al. 2008). From hydrostatic equilibrium, we have $P = \rho g H_p$. Assuming now the equation of state of a perfect gas, we then derive $H_p \propto T/g$. The sound speed is given by the relation $c_s^2 = \Gamma_1 P/\rho$. Accordingly, using again the perfect gas equation, we then have $c_s^2 \propto T$. From these simplifications, we can simplify Eq. (73) as:

$$\mathcal{P} \propto \omega_{\text{osc}}^2 F_{\text{kin}} T^3 g^{-4} . \quad (75)$$

In the framework of the mixing-length approach, it can be shown that F_{kin} is roughly proportional to the convective flux F_c . Indeed, in this framework, the eddies are accelerated by the buoyancy force over a distance equal to the mixing-length $\Lambda = \alpha H_p$ where α is the mixing-length parameter. Accordingly, the kinetic energy of the eddies, E_{eddy} , is given by (see the lecture notes by Bohm-Vitense 1989)

$$E_{\text{eddy}} \equiv \frac{3}{2} \rho u_0^2 \Lambda^3 = g (\Delta\rho \Lambda^3) \Lambda \quad (76)$$

where $\Delta\rho$ is the difference between the density of the eddy and its surroundings. In the Boussinesq approximation, the perturbation of the equation of state gives:

$$\frac{\Delta\rho}{\rho} \propto \frac{\Delta T}{T} \quad (77)$$

where ΔT is the difference between the temperature of the eddy and its surrounding. Now, the convective flux (also referred to as the enthalpy flux) is by definition the quantity:

$$F_c \equiv u_0 (\rho C_p \Delta T) \quad (78)$$

where $c_p = (\partial s / \partial \ln T)_p$. Finally, from the definition of Eq. (74) and the set of Eqs. (76)-(78), one derives $F_{\text{kin}} \propto g \Lambda / T F_c$ and, since $\Lambda \propto T/g$, we show finally that $F_{\text{kin}} \propto F_c$.

In the region where the driving is the most efficient, the total energy flux, F_{tot} , is no longer totally transported by convection (that is $F_c \langle F_{\text{tot}} \rangle$). However, in order to derive an expression that depends only on the surface parameters of the star, we will assume that all of the energy is transported by convection ; that is $F_c \approx F_{\text{tot}} = \sigma T_{\text{eff}}^4 \propto g (L/M)$ where σ is the Steffan's constant. Accordingly, Eq. (75) can be further simplified as:

$$\mathcal{P} \propto \omega_{\text{osc}}^2 T_{\text{eff}}^4 T^3 g^{-4} \approx \omega_{\text{osc}}^2 T_{\text{eff}}^7 g^{-4} , \quad (79)$$

⁵ for the sake of simplicity we assume here an isotropic medium, accordingly the flux of kinetic energy is the same in any direction

where we have assumed $T = T_{\text{eff}}$.

Let now defines $\nu_{\text{max}} = \omega_{\text{osc}}^{\text{max}}/2\pi$ the peak frequency associated with \mathcal{P} . This characteristic frequency can be estimated according to:

$$\nu_{\text{max}} \approx u_0/\Lambda \quad (80)$$

where the quantity u_0/Λ is estimated in the layer where u_0 is maximum. Using similar simplifications as used previously for \mathcal{P} , we can show that

$$\nu_{\text{max}} \propto g (T_{\text{eff}}/\bar{\rho})^{1/3}, \quad (81)$$

where $\bar{\rho}$ is the mean density at the photosphere. We assume that $\bar{\rho}$ is equal to the star mean density, that is $\bar{\rho} \approx M/R^3 \propto g/R$. Accordingly, we then derive from Eq. (79) and Eq. (81):

$$\mathcal{P}_{\text{max}} \propto (T_{\text{eff}}^4)^{23/12} g^{-3} M^{1/3}, \quad (82)$$

where M is the stellar mass. For main sequence stars lying in the domain where solar-like oscillations are expected, $M^{1/3}$ varies very slowly such that it can be ignored in Eq. (82). Then, Eq. (82) can finally be simplified as:

$$\mathcal{P}_{\text{max}} \propto (T_{\text{eff}}^4)^2 g^{-3}. \quad (83)$$

We now clearly see from Eq. (83) that \mathcal{P}_{max} as expected increases with increasing $F_{\text{tot}} = \sigma T_{\text{eff}}^4$ and decreases with increasing g .

10.2 Mode surface velocity

Prior to the CoRoT mission, only crude and indirect derivations of the averaged mode linewidth had been proposed for a few stars (see Kjeldsen et al. 2005; Fletcher et al. 2006; Kjeldsen et al. 2008). However, for the majority of solar-like pulsators observed so far from the ground in Doppler velocity, such measurements are not available, only the maximum of the mode surface velocity (V_{max} hereafter) is in general accessible. For the numerous solar-like pulsators observed from the ground, we must compute the mode surface velocity according to Eq. (13), which requires the knowledge of not only \mathcal{P} but also of the mode damping rates ($\eta = \pi \Gamma$).

Houdek et al. (1999) have computed η for a large set of main sequence models. Using Balmforth (1992a)'s formulation of stochastic excitation, they have also computed the mode excitation rates (\mathcal{P}). From their theoretical computations of \mathcal{P} and $\Gamma = \eta/\pi$, they have derived v_s according to Eq. (13). Their theoretical calculations for V_{max} result in a scaling law of the form $(L/M)^\beta$ with an exponent $\beta=1.5$ (see Houdek et al. 1999).

We have plotted in Fig. 11 the quantity V_{max} associated with the solar-like pulsators observed so far in Doppler velocity. Clearly, V_{max} increases as $(L/M)^\beta$ where the exponent $\beta \simeq 0.7$. A similar scaling law with the exponent $\beta = 1$ was earlier derived by Kjeldsen & Bedding (1995) from the theoretical calculations

by Christensen-Dalsgaard & Frandsen (1983). Houdek et al. (1999)’s scaling law significantly over-estimates the mode amplitudes in F-type stars. For instance for Procyon ($T_{\text{eff}} \simeq 6480$ K, $L \simeq 6.9 L_{\odot}$ and $L/M \simeq 4.6$), this scaling law over-estimates V_{max} by a factor ~ 4 .

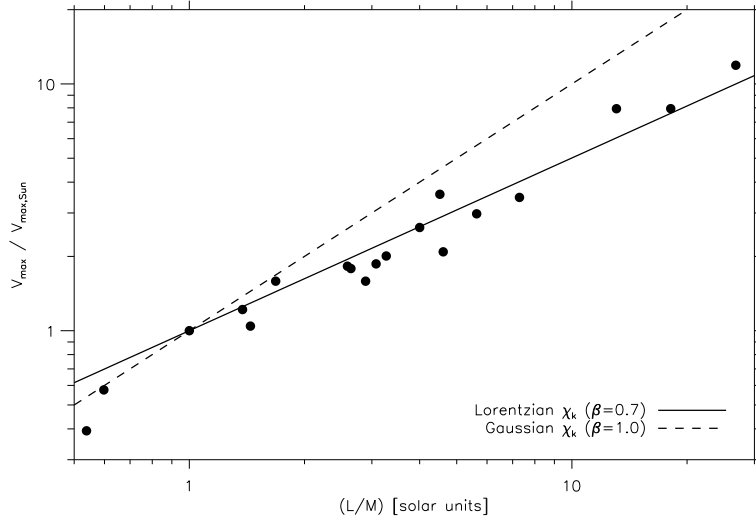


Fig. 11. Ratio between V_{max} the maximum of the mode velocity relative to the observed solar value ($V_{\text{max}}^{\odot} = 25.2$ cm/s for $\ell = 1$ modes, see Kjeldsen et al. 2008). Filled dots correspond to the stars for which solar-like oscillations have been detected in Doppler velocity (see a detailed list of references in Bedding & Kjeldsen 2007). The lines – except the dot-dashed line – correspond to the power laws obtained from the predicted scaling laws for \mathcal{P}_{max} and estimated values of the damping rates η_{max} (see text for details). Results for two different eddy time-correlation functions, χ_k , are presented: Lorentzian χ_k (solid line) and Gaussian χ_k (dashed line).

Samadi et al. (2007) have derived V_{max} using mode damping rates computed by Houdek et al. (1999) and the different scaling laws found for $\mathcal{P}_{\text{max}} \propto (L/M)^{\alpha}$. They also found that V_{max} scales as $(L/M)^{\beta}$. This is not surprising since \mathcal{P}_{max} varies as $(L/M)^{\alpha}$. Furthermore, the exponent β is found to depend significantly on the choice of χ_k : $\beta = 0.7$ for a Lorentzian χ_k and $\beta = 1$ for a Gaussian χ_k . As shown in Fig 11, the best agreement with the observations is found when a Lorentzian χ_k is assumed. On the other hand, assuming a Gaussian χ_k results in a larger exponent β . When theoretical mode amplitudes are calibrated with respect to the solar mode amplitudes, calculations based on a Gaussian χ_k over-estimate the amplitudes of solar-like pulsators significantly more luminous than the Sun.

Theoretical calculations by Houdek et al. (1999) assume a Gaussian χ_k . Then according to Samadi et al. (2007)’s results, the too large value found for β by

Houdek et al. (1999) can partially be explained by the use of a Gaussian χ_k . However, according to Houdek (2006), their too high value of β might be explained essentially by the mode damping rates that could be under-estimated by a factor ~ 1.8 .

11 Discussion and perspectives

The way mode excitation by turbulent convection is modeled is still very simplified. As discussed below, several approximations must be improved, some assumptions or hypothesis must be removed.

As seen in Sect. 5.2, the driving efficiency crucially depends on the eddy time-correlation (χ_k). Current models assume that χ_k varies with ω in the same way at any length scale. At the length scale of the energy bearing eddy, there are some strong indications that χ_k is Lorentzian rather than Gaussian. However, at smaller scale, it is not yet clear what is the correct description for χ_k . Use of more realistic 3D simulations would be very helpful to represent the correct dynamic behavior of the small-scales.

Current theoretical models that include the entropy fluctuations in the driving assume that the entropy fluctuations behave as a passive scalar (see Sect. 4.3). As a consequence, cross terms between \mathcal{S}_R and \mathcal{S}_S vanish. This is a *strong hypothesis* that is unlikely to be valid in the super-adiabatic part of the convective zone where driving by the entropy is important. Indeed, the super-adiabatic layer is a place where the radiative losses of the eddies are important because of the optically thin layers. Assuming that the entropy (or equivalently the temperature) is diffusive (Eq. (33)) is no longer valid. Furthermore, departure from incompressible turbulence is the largest in that layer and, accordingly, the cross terms between \mathcal{S}_R and \mathcal{S}_S no longer vanish (see SG). Therefore, the passive scalar assumption is not valid in the super-adiabatic layers. To avoid this assumption, one needs to include the radiative losses in the modeling.

One other approximation concerns the spatial separation between the modes and the contributing eddies. This approximation is less valid in the super-adiabatic region where the turbulent Mach number is no longer small, in particular for high ℓ order modes. This spatial separation can however be avoided if the kinetic energy spectrum associated with the turbulent elements ($E(k)$) is properly coupled with the spatial dependence of the modes (work in progress).

The CoRoT mission, launched 27 December, is precise enough to detect solar-like oscillations with amplitudes as low as the solar p modes (Michel et al. 2008). Furthermore, thanks to its long term (up to 150 days) and *continuous* observations, it is possible with CoRoT to resolve solar-like oscillations, and hence to measure not only the mode amplitudes but also *directly* the mode linewidths (see e.g. Appourchaux et al. 2008). Similarly as in the case of the Sun, it is now possible with CoRoT to derive direct constraints on \mathcal{P} for stars with different characteristics: evolutionary status, effective temperature, gravity, chemical composition, magnetic field, rotation, surface convection, ... etc. We emphasize

below some physical processes and conditions that we expect to address thanks to the CoRoT data.

Some solar-like pulsators are young stars that show rather strong activity (e.g. HD 49933, HD 181420, HD 175726, HD 181906, ...). A high level of activity is often linked to the presence of strong magnetic field. Effects of the magnetic field are not taken into account in the calculation of the mode excitation rates. A strong magnetic field can more or less inhibit convective transport (see e.g. Proctor & Weiss 1982; Vögler et al. 2005). Furthermore, as shown by Jacoutot et al. (2008a), a strong magnetic field can significantly change the way turbulent kinetic energy is spatially distributed and leads to a less efficient driving of the acoustic modes. In that framework, the CoRoT target HD 175726 is probably an interesting case. Indeed, this star shows both a particularly high level of activity and solar-like oscillations with amplitudes significantly lower than expected (Mosser et al. 2009).

Young and active stars rotate usually faster than the Sun. As shown recently by Belkacem et al. (2009a), the presence of rotation introduces additional sources of driving. However, in the case of a moderate rotator such as HD 49933, these additional sources of driving remain negligible compared to the Reynolds stress and the entropy source term. On the other hand, the presence of rotation has an indirect effect on mode driving through the modification of the mode eigenfunctions. An open issue is: will the CoRoT or the Kepler mission be able to test the expected effect of rotation (see Belkacem et al. 2009a)?

Solar-like oscillations have now been firmly detected in several red giant stars, from both Doppler velocity measurements (see the review by Bedding & Kjeldsen 2006) as well as from space based photometry measurements (Barban et al. 2007; de Ridder et al. 2006). More recently, detection of solar-like oscillations by CoRoT in a huge number of red giant stars has been announced by de Ridder et al. (2009). Why look at solar-like oscillations in red giant stars? Toward the end of their lives, stars like the Sun greatly expand to become giant stars. A consequence of this great expansion, is the existence of a very dilute convective envelope. A low density favors a vigorous convection, hence higher Mach numbers (M_t). The theoretical models of stochastic excitation are strictly valid in a medium where M_t is – as in the Sun and α Cen A – rather small. Hence, the higher M_t , the more questionable the different approximations and the assumptions involved in the theory. Hence, red giant stars allow us to test the theory of mode driving by turbulent in more extreme conditions.

Finally, most of theories of stochastic excitation are developed for radial modes only. Dolginov & Muslimov (1984), GMK and Belkacem et al. (2008) have considered the non-radial case. There are interesting applications of such non-radial formalisms, for instance the case of solar g modes (Belkacem et al. 2009b), but also g modes in massive stars that can in principle be excited in their central convective zones (Samadi et al. 2009a).

Acknowledgment

I am very grateful to Marie-Jo Goupil and Kévin Belkacem for their valuable comments and advise. I am indebted to J. Leibacher for his careful reading of the manuscript. I am grateful to the organizers of the CNRS school of St-Flour for their invitation and I thank the CNRS for the financial support.

Bibliography

- Abdella, K. & McFarlane. 1997, *J. Atm Phys*, 54, 1850
- Appourchaux, T., Michel, E., Auvergne, M., et al. 2008, *A&A*, 488, 705
- Balmforth, N. J. 1992a, *MNRAS*, 255, 639
- Balmforth, N. J. 1992b, *MNRAS*, 255, 632
- Barban, C., Matthews, J. M., de Ridder, J., et al. 2007, *A&A*, 468, 1033
- Batchelor, G. K. 1970, *The theory of homogeneous turbulence* (University Press)
- Baudin, F., Samadi, R., Goupil, M.-J., et al. 2005, *A&A*, 433, 349
- Bedding, T. R. & Kjeldsen, H. 2006, *Memorie della Societa Astronomica Italiana*, 77, 384
- Bedding, T. R. & Kjeldsen, H. 2007, *Communications in Asteroseismology*, 150, 106
- Belkacem, K., Mathis, S., Goupil, M. J., & Samadi, R. 2009a, in press ([astro-ph/0909.148](#))
- Belkacem, K., Samadi, R., Goupil, M.-J., & Dupret, M.-A. 2008, *A&A*, 478, 163
- Belkacem, K., Samadi, R., Goupil, M. J., et al. 2009b, *A&A*, 494, 191
- Belkacem, K., Samadi, R., Goupil, M. J., & Kupka, F. 2006a, *A&A*, 460, 173
- Belkacem, K., Samadi, R., Goupil, M. J., Kupka, F., & Baudin, F. 2006b, *A&A*, 460, 183
- Benomar, O., Baudin, F., Campante, T. L., et al. 2009, *A&A*, 507, L13
- Böhm-Vitense, E. 1958, *Zeitschr. Astrophys.*, 46, 108
- Bohm-Vitense, E. 1989, *Introduction to stellar astrophysics*, Vol. 3 (Cambridge University Press)
- Chaplin, W. J. & Basu, S. 2008, *Solar Physics*, 36
- Chaplin, W. J., Elsworth, Y., Isaak, G. R., et al. 1998, *MNRAS*, 298, L7
- Chaplin, W. J., Houdek, G., Elsworth, Y., et al. 2005, *MNRAS*, 360, 859
- Christensen-Dalsgaard, J. & Frandsen, S. 1983, *Solar Physics*, 82, 469
- Cowling, T. G. 1941, *MNRAS*, 101, 367
- de Ridder, J., Barban, C., Baudin, F., et al. 2009, *Nature*, 459, 398
- de Ridder, J., Barban, C., Carrier, F., et al. 2006, *A&A*, 448, 689
- Deubner, F. L. 1975, *A&A*, 44, 371
- Dolginov, A. Z. & Muslimov, A. G. 1984, *Ap&SS*, 98, 15
- Fletcher, S. T., Chaplin, W. J., Elsworth, Y., Schou, J., & Buzasi, D. 2006, *MNRAS*, 824
- Georgobiani, D., Stein, R. F., & Nordlund, Å. 2006, in *Astronomical Society of the Pacific Conference Series*, Vol. 354, *Solar MHD Theory and Observations: A High Spatial Resolution Perspective*, ed. J. Leibacher, R. F. Stein, & H. Uitenbroek, 109

- Goldreich, P. & Keeley, D. A. 1977a, *ApJ*, 211, 934
- Goldreich, P. & Keeley, D. A. 1977b, *ApJ*, 212, 243 (GK)
- Goldreich, P., Murray, N., & Kumar, P. 1994, *ApJ*, 424, 466 (GMK)
- Gough, D. 1976, in *Lecture notes in physics*, Vol. 71, *Problems of stellar convection*, ed. E. Spiegel & J.-P. Zahn (Springer Verlag), 15
- Gough, D. O. 1977, *ApJ*, 214, 196
- Gryanik, V. & Hartmann, J. 2002, *J. Atmos. Sci.*, 59, 2729
- He, G.-W., Rubinstein, R., & Wang, L.-P. 2002, *Physics of Fluids*, 14, 2186
- Houdek, G. 2006, in *ESA Special Publication*, Vol. 624, *Proceedings of SOHO 18/GONG 2006/HELAS I, Beyond the spherical Sun*, Published on CDROM, p. 28.1
- Houdek, G. 2008, *Communications in Asteroseismology*, 157, 137
- Houdek, G., Balmforth, N. J., Christensen-Dalsgaard, J., & Gough, D. O. 1999, *A&A*, 351, 582
- Jacoutot, L., Kosovichev, A. G., Wray, A., & Mansour, N. N. 2008a, *ApJ*, 684, L51
- Jacoutot, L., Kosovichev, A. G., Wray, A. A., & Mansour, N. N. 2008b, *ApJ*, 682, 1386
- Kjeldsen, H. & Bedding, T. R. 1995, *A&A*, 293, 87
- Kjeldsen, H., Bedding, T. R., Arentoft, T., et al. 2008, *ApJ*, 682, 1370
- Kjeldsen, H., Bedding, T. R., Butler, R. P., et al. 2005, *ApJ*, 635, 1281
- Kolmogorov, A. N. 1941, *Dokl. Akad. Nauk SSSR*, 30, 299
- Kupka, F. & Robinson, F. J. 2007, *MNRAS*, 374, 305
- Ledoux, P. & Walraven, T. 1958, in *Handbuch der Physik*, ed. F. S., Vol. 51 (Springer-Verlag (New York)), 353
- Leibacher, J. W. & Stein, R. F. 1971, *Astrophys. Lett.*, 7, 191
- Lesieur, M. 1997, *Turbulence in fluids* (Kluwer Academic Publishers)
- Libbrecht, K. G. 1988, *ApJ*, 334, 510
- Lighthill, M. J. 1952, *Proc. R. Soc. Lond.*, A211, 564
- Michel, E., Baglin, A., Auvergne, M., et al. 2008, *Science*, 322, 558
- Mosser, B., Michel, E., Appourchaux, T., et al. 2009, *A&A*, 506, 33
- Musielak, Z. E., Rosner, R., Stein, R. F., & Ulmschneider, P. 1994, *ApJ*, 423, 474
- Nordlund, Å. & Stein, R. F. 1999, in *Astronomical Society of the Pacific Conference Series*, Vol. 173, *Stellar Structure: Theory and Test of Connective Energy Transport*, ed. A. Gimenez, E. F. Guinan, & B. Montesinos, 91
- Nordlund, Å. & Stein, R. F. 2001, *ApJ*, 546, 576
- Oboukhov, A. 1941, *Dokl. Akad. Sci. Nauk SSSR*, 32, 22
- Osaki, Y. 1990, in *Lecture Notes in Physics*, Berlin Springer Verlag, Vol. 367, *Progress of Seismology of the Sun and Stars*, ed. Y. Osaki & H. Shibahashi, 75
- Proctor, M. R. E. & Weiss, N. O. 1982, *Reports of Progress in Physics*, 45, 1317
- Roca Cortés, T., Montañés, P., Pallé, P. L., et al. 1999, in *Astronomical Society of the Pacific Conference Series*, Vol. 173, *Stellar Structure: Theory and Test of Connective Energy Transport*, ed. A. Gimenez, E. F. Guinan, & B. Montesinos, 305

- Rosenthal, C. S., Christensen-Dalsgaard, J., Nordlund, Å., Stein, R. F., & Trampedach, R. 1999, *A&A*, 351, 689
- Samadi, R., Belkacem, K., Goupil, M.-J., Dupret, M.-A. and Brun, A., & Noels, A. 2009a, submitted to *Ap&SS*
- Samadi, R., Belkacem, K., Goupil, M. J., Dupret, M.-A., & Kupka, F. 2008, *A&A*, 489, 291
- Samadi, R., Georgobiani, D., Trampedach, R., et al. 2007, *A&A*, 463, 297
- Samadi, R. & Goupil, M. J. 2001, *A&A*, 370, 136 (SG)
- Samadi, R., Goupil, M. J., & Lebreton, Y. 2001, *A&A*, 370, 147
- Samadi, R., Kupka, F., Goupil, M. J., Lebreton, Y., & van't Veer-Menneret, C. 2006, *A&A*, 445, 233
- Samadi, R., Ludwig, H., Belkacem, K., et al. 2009b, *A&A*, in press (astro-ph/0910.4037)
- Samadi, R., Ludwig, H., Belkacem, K., Goupil, M.-J., & Dupret, M. 2009c, *A&A*, in press (astro-ph/0910.4027)
- Samadi, R., Nordlund, Å., Stein, R. F., Goupil, M. J., & Roxburgh, I. 2003a, *A&A*, 404, 1129
- Samadi, R., Nordlund, Å., Stein, R. F., Goupil, M. J., & Roxburgh, I. 2003b, *A&A*, 403, 303
- Spiegel, E. 1962, *J. Geophys. Res.*, 67, 3063
- Stein, R., Georgobiani, D., Trampedach, R., Ludwig, H.-G., & Nordlund, Å. 2004, *Solar Physics*, 220, 229
- Stein, R. F. 1967, *Solar Physics*, 2, 385
- Stein, R. F. & Nordlund, Å. 2001, *ApJ*, 546, 585
- Ulrich, R. K. 1970, *ApJ*, 162, 993
- Unno, W. & Kato, S. 1962, *PASJ*, 14, 417
- Unno, W., Osaki, Y., Ando, H., Saio, H., & Shibahashi, H. 1989, *Nonradial oscillations of stars* (Tokyo: University of Tokyo Press, 1989, 2nd ed.)
- Vögler, A., Shelyag, S., Schüssler, M., et al. 2005, *A&A*, 429, 335
- Xiong, D. R., Cheng, Q. L., & Deng, L. 2000, *MNRAS*, 319, 1079